Universidad Carlos III de Madrid
www.uc3m.es

Bachelor's Degree in Biomedical Engineering

Bachelor Thesis

Fluorescence Endoscopy In-vivo based on Fiber-bundle Measurements

Author: Blanca Zufiria Gerbolés

Tutor: Jorge Ripoll Lorenzo

Co-tutor: Alicia Arranz De Miguel

Universidad Carlos III de Madrid
CBM Severo Ochoa
SaludMadrid
Hospital General Universitario Gregorio Marañón
Comunidad de Madrid

AKNOWLEDGEMENTS

I wish to express my gratitude to the following people for their support during this project.

First I am grateful to my tutor, Jorge Ripoll Lorenzo, for giving me the opportunity to work on this project that has been an amazing experience, for his support and for being available whenever I needed, inverting so much time in my project. It was a pleasure working with him.

To my co-tutor, Alicia Arranz, for her time and attention all the time, for their kindness and for her motivation on this project. I have acquired incredible knowledge and experience during all my stays in the laboratory.

To Guillermo Vizcaíno for his dedication and perfectionism to make my project so professional.

To Diana Bocancea for investing her time in teaching me and in obtaining excellent results.

Thank you to all my friends including the ones I have done at the university, Marina and Isa, your friendship has been all for me these years. To Roslancas for being my greatest support in the day to day trusting in me every moment.

To Daniel that lived this project with me. Thank you for your smile and joy, for being a good listener and for helping me in any situation.

Finally thank you so much to my family for their trust during all those months, for make me so happy and for being so proud of me.

ABSTRACT

High-resolution imaging techniques have become important for the determination of the cellular organization that is coupled to organ function. In many cases the organ can be viewed without the need of ionizing radiation techniques in an easier and achievable way. This is the case of the gastrointestinal tract, and organ that can be directly accessed with endoscopy without the need of an invasive procedure. Many studies on diseases of the Gastrointestinal Tract are currently under way due to their large impact in human health.

Mice and rats have been used for the study of these diseases, and in particular cancer, due to their similar anatomy and physiology with humans and their easy handling. The main objective of this project is to design a fluorescence high resolution endoscope test it in mice, without and with cancer previously induced in the large intestine, imaging the cellular organization of the colon. Access to the colon of the mouse takes place through the use of a fiber-optic bundle that redirects the light coming from a led to produce fluorescence and detect it back through the fiber bundle.

This project has been done at the Universidad Carlos III de Madrid where the design of the fluorescence high-resolution endoscope for small animals took place; and in collaboration with the Centro de Biología Molecular Severo Ochoa de Madrid where the in-vivo testing in mice and laboratory protocols for further diagnosis and validation of the endoscope were performed.

Contents

1. INTRODUCTION 14

1.1. Motivation 14

1.2. Gastrointestinal track 15

1.3. Endoscopy 17

1.3.1. Fiber-optic endoscopy 19

1.4. Fluorescence microscopy 21

1.4.1. Selective Plane Illumination Microscopy (SPIM) 22

1.4.2. Tissue clearing methods 25

2. OBJECTIVES 27

2.1. Development of a high resolution fiber-optic fluorescence endoscope 27

2.1.1. In-vivo application 27

2.1.2. In vitro and microscopy validation 28

3. MATERIALS AND METHODS 29

3.1. Fiber-optic endoscope components and system assembly 29

3.1.1. Near-Infrared Fluorescence camera 29

3.1.2. Illumination system 30

3.1.3. Lenses and objective 31

3.1.3.1. Objective 31

3.1.3.2. Biconvex lens 31

3.1.3.3. Aspheric lens 32

3.1.4. Filters and dichroic mirror 32

3.1.4.1. Excitation filter 33

3.1.4.2. Dichroic mirror and emission filter 33

3.1.5. Optical fiber bundle 35
3.1.5.1. GRIN lens 37
3.1.6. Final system assembly 38
3.2. Fiber-optic endoscope control with LabVIEW program 40
3.3. Calibration protocol 41
3.4. Resolution 43
3.5. In-vivo test 45
3.6. In-vitro test 47
3.7. 3D image acquisition with SPIM microscope 47
3.7.1. CUBIC clearing protocol 48
3.7.1.1. Solutions 48
3.7.1.2. Protocol for mouse colon 49
3.7.2. SPIM image acquisition 50
3.8. Image processing 52
4. RESULTS AND DISCUSSION 53
4.1. Optical fibers 53
4.1.1. Resolution 54
4.2. In-vivo results 55
4.3. In-vitro and Selective Plane Illumination Microscope results 57
5. CONCLUSIONS 61
6. FUTURE WORK 63
PROJECT COSTS 64
ANNEX 67
LabVIEW Program 67
Reference Sheet 70
Publications 72

BIBLIOGRAPHY 77

List of figures

Figure 1. Gross anatomy of the human and the mouse gastrointestinal track *(from [5])*.....16

Figure 2. The structure of the large intestine (colon) crypt formed by different types of cells *(from [6])* 16

Figure 3. Components of and endoscopy system *(from [8])* 18

Figure 4. Inserting tube of a fiber-optic endoscope *(from [10])* 19

Figure 5. A) Fiber bundle of a fiber-optic endoscope *(from [11])* ***B) Optical Fiber*** *(from [12])*.....20

Figure 6. SPIM fluorescence microscopy setup. The light sheet illumination (blue) and the objective detection (green) perpendicular to each other with the sample in the focal pane of intersection *(from [13])* 23

Figure 7. a) Low transparency through absorbing pigments; b) Low transparency due to effective scattering at surfaces with changing refractive index; c) High transparency after equalization of refractive indices *(from [14])* 25

Figure 8. A mouse brain before (left) and after (right) clearing with amino alcohols using CUBIC clearing protocol *(from [15])* 26

Figure 9. Scheme of the fiber-optic endoscope system.....29

Figure 10. LED used in the endoscopy system......30

Figure 11. 10X Olympus Plan Achromat Objective, 0.25 NA, 10.6 mm WD *(from [19])*.....31

Figure 12. Aspheric lens. A. Aspheric lens used for our system assembly and B. Sketch of aspheric lens *(from [18])* 32

Figure 13. A) Light path through excitation/emission filters and dichroic mirror B) Spectrum of the Fluorescence Filter Combination and Acriflavine. 35

Figure 14. Fijikura image fiber cross section structure *(from [23])*.....36

Figure 15. A) SMA connector B) Fiber bundles with (left) and without (right) GRIN lens and SMA connector assembly 36

Figure 16. Rays path through GRIN lens *(from [24])*.....37

Figure 17. Fiber bundle without (upper) and with (down) GRIN lens. 38

Figure 18. Fiber bundle endoscope A) Open box with all components and B) Close box. 39

Figure 19. Interface of the fiber-optic endoscope LabVIEW program......40

Figure 20. Fiber–optic coupling where the fiber is threaded and the focusing wheel to focus the image. 41

Figure 21. Examples of imaging with the fiber-optic bundle. A) Poor focus B) Good focus C) Ideal Focus 42

Figure 22. A) USAF Test Target B) Set of group lines and numbers that determine the resolution *(from [28])* 43

Figure 23. Table of number of lines pairs/mm depending on the element and the group. *(from [28])*..44

Figure 24. Fiber-optic with GRIN lens placed on a foot and Test Target on the small engine. *44*
Figure 25. Normal control mice displayed normal colonic histology with an intact epithelium where crypts are well defined while in DSS we can observed that the epithelium has been destroyed and the crypt structure has disappeared *(from [30])* *45*
Figure 26. Testing the fluorescence fiber-optic endoscope in in-vivo (mouse) with the fiber bundle without GRIN lens. *46*
Figure 27. In-vitro test. A) Acriflavine at 0.01% of concentration (left) and fixed mouse intestines in PBS (right), and a petri dish (down) in which the experiment was performed B) Insertion of the optic fiber with the help of tweezers through the fixed mouse colon. *47*
Figure 28. Colon of a mouse seen with the fiber-optic endoscope in-vitro A) with GRIN lens and B) without GRIN lens *53*
Figure 29. Picture of the smallest set of lines of the test target obtained with the fiber-optic without GRIN lens *54*
Figure 30. Images of element 4 and group 2 of the Test Target taken in 0.02 cm increments starting at distance 0 cm. GRIN lens surface in contact with Test Target surface (first image) and moving far away until 0.42 cm, distance from GRIN lens to Test Target (last image). *55*
Figure 31. Colon of a mouse seen with the fiber-optic endoscope in-vivo. A) Tumor-free area in which we can appreciate the crypt structure of the intestine. B) Tumor affected area in which we can see how the crypt structure disappears. *56*
Figure 32. Colon of a healthy mouse seen with the endoscope in-vivo *56*
Figure 33. Colon of a healthy mouse seen with the endoscope in-vitro in which we can appreciate the crypt structure of the colon tissue. *57*
Figure 34. Colon of a mouse seen with the fiber-optic endoscope in-vitro in which we can appreciate the crypt structure of the colon tissue. *58*
Figure 35. Colon of a mouse in which cancer was induced analyzed with the fiber-optic endoscope in-vivo (before extraction with the mouse alive), in-vitro (after extraction) and under SPIM. *58*
Figure 36. Colon of a mouse. A) Tumor-free fragment (right) and tumor fragment (left) imaged with the fluorescence fiber-optic endoscope in vivo B) Tumor-free fragment (left) and tumor fragment (right) seen under SPIM with a 2x detection objective and 3D reconstructed with ImageJ. *59*
Figure 37. Fragments of the colon of a mouse seen under SPIM with a 5x detection objective. A) Tumor-free fragment in which we can appreciate the crypt structure and B) Tumor fragment in which we cannot see any tissue structure. *60*
Figure 38. Control Window of the LabVIEW program *67*
Figure 39. Terminal Window of the LabVIEW program *68*
Figure 40. Terminal Window of the LabVIEW program *69*

List of tables

Table 1. Dichroic mirror specifications *(from [21])*.....*34*

Table 2. Two different magnification objectives available in the setup of the SPIM microscope at Medical Imaging Laboratory, Hospital Gregorio Marañon......*51*

Table 3. Excitation lasers and emission filters available in the setup of the SPIM microscope at Medical Imaging Laboratory, Hospital Gregorio Marañón. In the third column fluorescent labeling and dyes with matching excitation and emission spectra.....*52*

Table 4. Endoscope components asscociated costs.....*64*

Table 5. Technical equipment associated costs.....*65*

Table 6. Laboratory material associated costs.....*66*

Table 7. Human resources associated costs......*66*

Table 8. Total Project cost.....*66*

1. INTRODUCTION

1.1. Motivation

Understanding the Gastrointestinal tract has been an important field of study for many scientist and researchers. Colorectal cancer, a type of cancer developed in the colon or in the rectum, is the third most common cause of death in men and women and also the second most common cause of death when numbers for both men and women are combined [1]

The early detection of colorectal cancer is crucial for the diagnosis and curation, increasing significantly the probability of survival. Regular screening, looking for cancer or precancer indicators before any symptom of the disease, can prevent many cases of colorectal cancer by finding and removing certain types of cells before they can develop into cancer. If cancer was found early before it has spread or developed, the survival of 5 years is about 90%, much higher than when detected at later stages. Different techniques has been used for screening and detecting this kind of cancer and endoscopy has become one of the most important ones for the prevention, early detection, diagnosis, and treatment of cancer. It is a non-harmful imaging technique and provide clinicians with additional information regarding about color, surface texture and other characteristics that cannot been seen with other imaging techniques such as X-rays and MRI [2]

New endoscopes have been developed for testing in animals such as mice to accelerate the diagnosis of colorectal cancer and make it more real and similar to humans. Many experiments for colorectal cancer are taking place today by inducing this cancer in rodents. Scientist and researchers rely on rats and mice for several reasons. On one hand, their small size is appropriate for breeding and handling, they are relatively easy to maintain and they adapt well to new environments. They also have a very similar human immune system as well as a similar human genome.

Mice and rats reproduce quickly and they have a high number of offspring with a short gestation period (19-21 days) and also a short lifespan of two to three years so several generations can be studied in relatively short periods of time [3].

Since their genetic, biological and behavior characteristics resembles those of humans and those similarities have become even stronger by genetic modifications, 'transgenic mice', they are efficient for research avoiding studies in humans. In particular, the gastrointestinal track is similar in mice. This allow us to increase the understanding of carcinogenesis, tumors and the impact of specific molecular events on the colon.

Colorectal cancer can be induced in mice in the gastrointestinal tract for further study of treatments that could be applied in humans. During this project we developed a high quality endoscopy system that uses fluorescence in order to study colorectal cancer in mouse large intestine.

1.2. Gastrointestinal track

The GI consists on a long tube inside the animal, with the mouth as the opening at the anterior end and the anus as the opening at the posterior end. The rodent digestive system has two main differences with respect to human digestive system. First, rodents do not have a gallbladder because they do not usually take large amount of fatty foods. Secondly, they have an enlarged large intestine, namely, the cecum that helps them to digest the grains and seeds they intake [4]

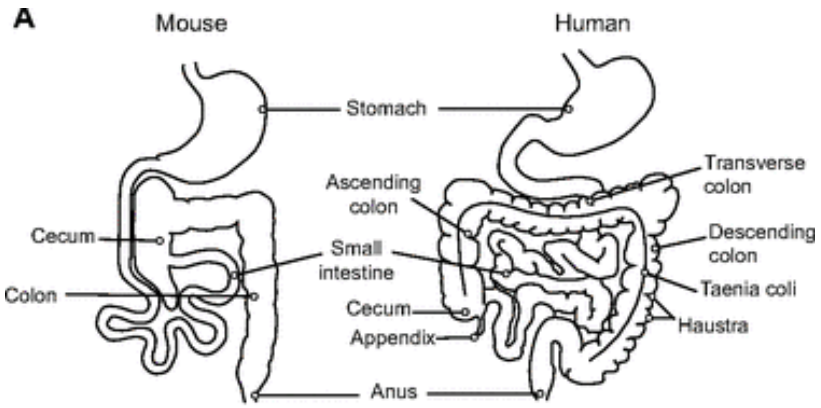

Figure 1. Gross anatomy of the human and the mouse gastrointestinal track *(from [5])*

The advantage of the GI is that it can be accessed directly with an endoscope avoiding invasive techniques. During this project, we have focused on the rectus and the colon in which colorectal cancer was induced and that can be reached easily with our endoscope. The goal is to image the texture of the mouse large intestine that is characterized by the crypt structure (Figure 2).

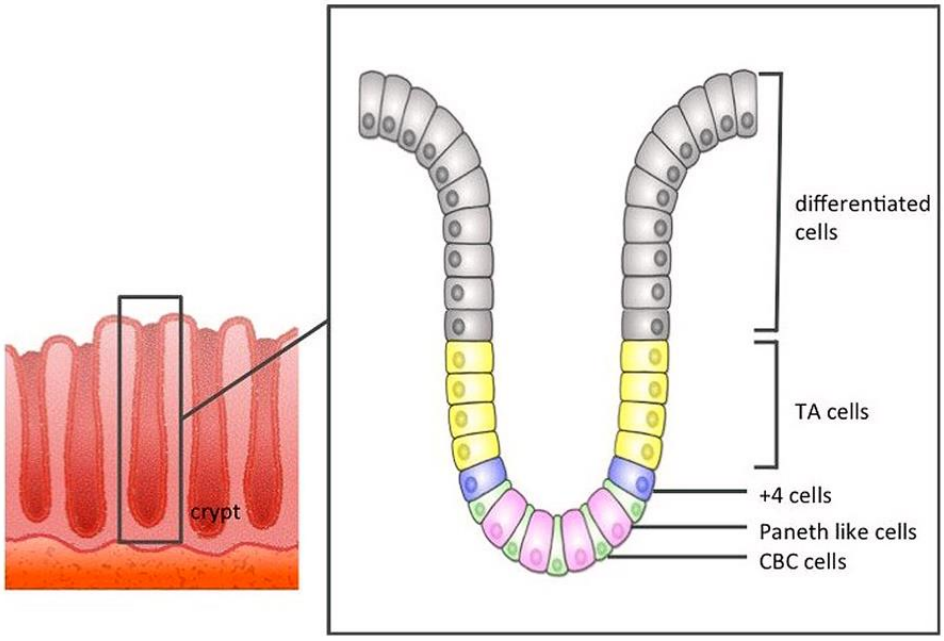

Figure 2. The structure of the large intestine (colon) crypt formed by different types of cells *(from [6])*

In the case of the large intestine (colon) a crypt is an intestinal gland (also crypt of Lieberkühn) that is composed of a structure of cells forming a microscopic tube shape with a central hole down the length of the tube (the crypt lumen).

The crypt structure in the colon of a mouse can be image with a fluorescent fiber-optic endoscope by inserting it into the large intestine where cells have previously been stained with a fluorescent reporter.

1.3. Endoscopy

Endoscopy is a medical procedure that consists on looking inside the organs and cavities of the body using an instrument called endoscope that has to be previously disinfected. The difference with other techniques is that the endoscope is inserted directly into the organ or while for example X-ray or MRI obtain images from the exterior of the body. This technique allows to see real time images providing functional information while other imaging techniques such as X-ray or MRI provide only static information.

Endoscopes have been used during almost two centuries since 1806 when Phillip Bozzini developed the first one for the examination of canals and cavities of the human body. Antonin Jean Desormeaux was the first one on using an endoscope in a successful operation before the invention of electricity.

The discovery of electricity was an improvement for endoscopy because it allows the use of an external electric light source for the illumination of the cavities under inspection. This lead to the use of endoscopes in laparoscopy, an operation performed in the abdomen or pelvis through small incisions (usually 0.5–1.5 cm) with the aid of a camera, by Hans Christian Jacobeaus in 1910.

Karl Storz played a crucial role in the development of endoscopy in 1945 when he set out to introduce very bright but cold light into the body cavities at the same time of image transmission.

In 1957 Basil Hirschowitz and Larry Curtiss invented the first fiber-optic endoscope thereby achieving the high level of full spectrum illumination that was needed for detailed viewing, and color photography [7]. This endoscope uses fiber bundles to illuminate the cavity or organ and to capture the image.

An endoscope is composed of different parts that combined have the ability to acquire high quality images in color and in real time. The different parts that form an endoscope are the following:

- A rigid or flexible inserting tube that is placed inside the cavity we want to examine. The length and radius vary depending on the cavity in which is going to be inserted. Inside it we have the fiber bundles, the video signal wires and sometimes a biopsy channel.
- A light delivery system to illuminate the organ that usually is outside the body of inspection and directs the light from the source to the body through a light tube.
- An image acquisition system composed of lenses and a camera that transmits the image to a screen for visualization.

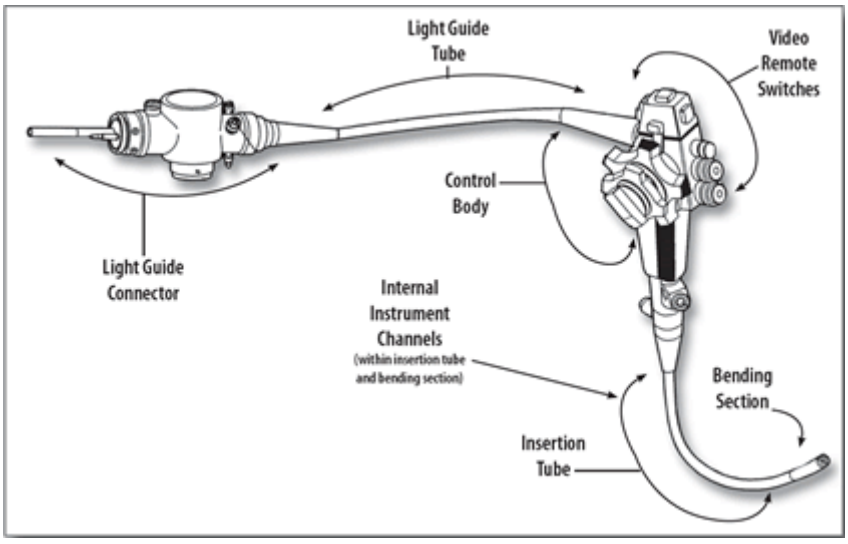

Figure 3. Components of and endoscopy system *(from [8])*

Endoscopes have been used for the inspection of different cavities and organs such as the gastrointestinal tract, urinary tract, respiratory tract, reproductive system, ear during surgery or the inspection of the fetus during pregnancy.

The main risks of using an endoscope are infection, over-sedation or perforation of the tissue but we have to remember that each of these occurs infrequently.

One of the most common endoscopies is colonoscopy in which the large intestine and the distal part of the small intestine are imaged by passing the flexible tube through the anus. Colonoscopy is very useful for the detection of cancer and other digestive diseases in which their early detection could be crucial for total recovery.

1.3.1. Fiber-optic endoscopy

Fiber-optic endoscopes use a flexible tube that consists of two or three main fiber bundles (Figure 5.A) each of which is formed up to 50,000 optical fibers. This optical fibers carry coherent light from one end of the fiber to the other by total internal refraction (Figure 5.B). One or two of the cables carry light down into the patient's body; another one carries reflected light (the image of the patient's cavity or organ) back up to the camera (Figure 4) [9]

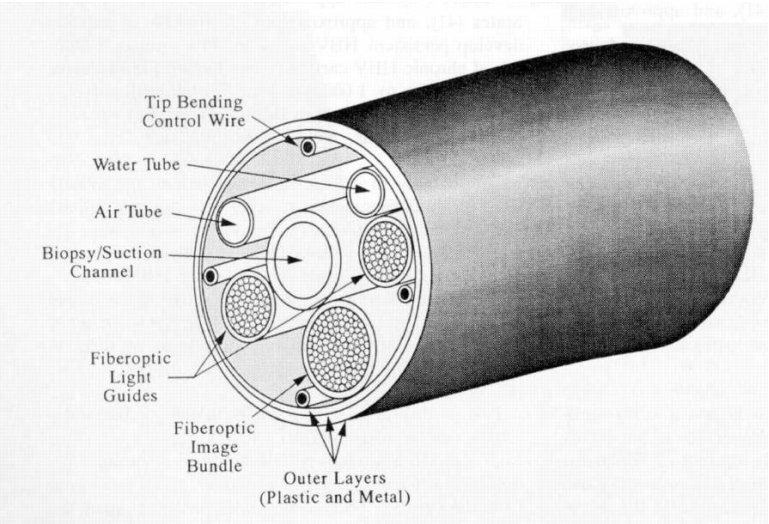

Figure 4. Inserting tube of a fiber-optic endoscope *(from [10])*

The advantage of these endoscopes is that they can be inserted in small cavities of the body that otherwise cannot be examined such as head and neck areas or arteries.

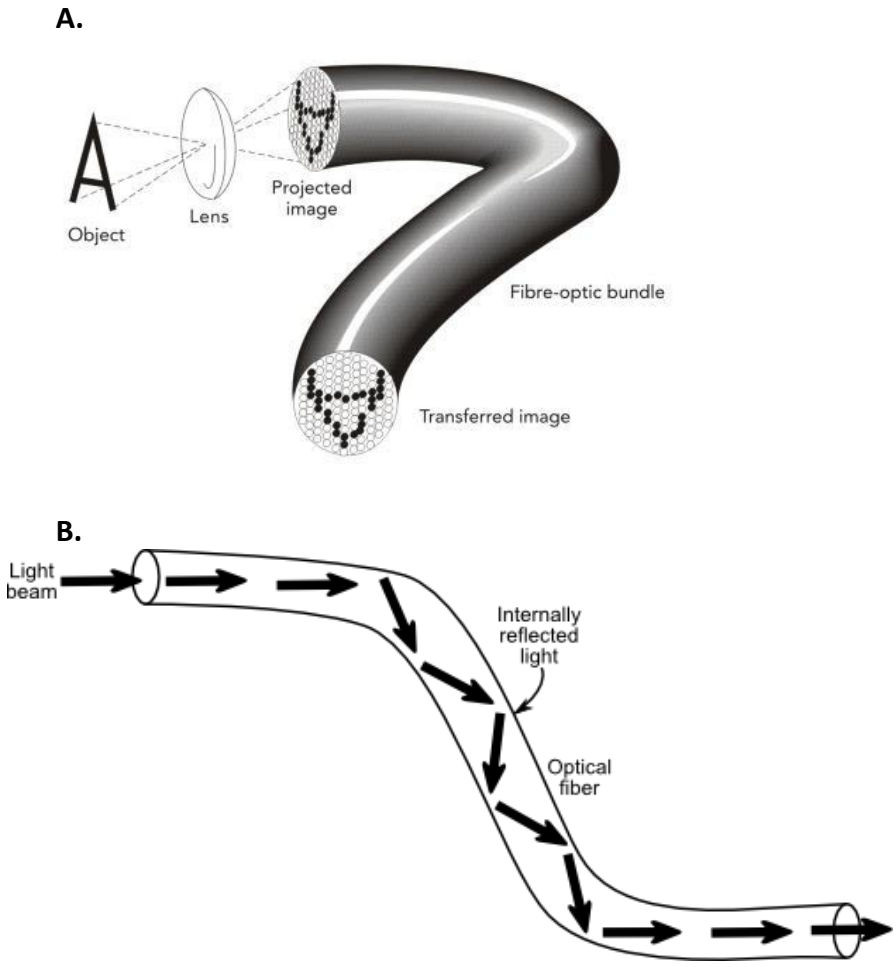

Figure 5. A) Fiber bundle of a fiber-optic endoscope *(from [11])* ***B) Optical Fiber*** *(from [12])*

These fiber-bundle endoscopes enable high-quality video for medical application and also provide us new options for in-vivo biological research and high resolution fluorescence imaging. They can be used in humans, animals or other living organism for different purposes including diagnosis, research and laboratory testing.

During this project we have developed a fluorescence fiber-optic endoscope for the inspection of the mouse large intestine. This endoscope differs from the common fiber-optic endoscope since it uses one single fiber bundle that transmits light and

captures images produced by fluorescence at the same time. Common fiber-optic endoscopes use two or three fiber bundles and more cables as described before.

1.4. Fluorescence microscopy

The basic optical microscopy technology uses a visible light source and an arrangement of lenses to magnify images of small samples. Although optical microscopy has played a fundamental role in cell and molecular biology and it has been available for over four centuries, fluorescence microscopy has been a breakthrough for microscopy. A fluorescence microscope is an optical microscope that uses fluorescence to create an image.

Fluorescence is a specific type of luminescence that characterizes substances, which are able to absorb energy in form of electromagnetic waves and, then, re-emit part of that energy as electromagnetic radiation with wavelength of lower energy that is measured by the detector. In fluorescence microscopy, the biological sample containing a fluorophore molecule, chemical compound that re-emit light upon light excitation, is illuminated through the objective lens with a narrow set of wavelengths of light. Between the photon absorption and emission there is a very short time delay depending on the lifetime of the excited state, which is usually in the range of tens of nanoseconds to hundreds of nanoseconds. The sample under study may naturally contain the fluorophore, be genetically modified to express it (in form of the Green Fluorescent Protein, GFP, and its variations) or it can be chemically manipulated by labelling specific cells and proteins with fluorescent stains through a process called immunofluorescence. Therefore, fluorescence has become a good choice as a diagnostic method. With the help of fluorescence, it is possible to access organs and cavities without the need of going through a surgery.

Fluorescence microscopy requires intense, near-monochromatic illumination. Four main types of light source are used, including xenon arc lamps or mercury-vapor lamps with an excitation filter, lasers, and high-power LEDs. Lasers are most widely used for more complex fluorescence microscopy techniques like confocal

microscopy and total internal reflection fluorescence microscopy while xenon lamps, mercury lamps, and LEDs with a dichroic excitation filter are commonly used for epi-fluorescence microscopes.

Its development had an important effect on biomedical research since it allowed scientists not only to observe normal physiological processes, which could be seen with other techniques, but also to detect and analyze several signals and to track them in real time.

There are different fluorescence microscope configurations and during this project we used an optical sectioning microscope termed light-sheet fluorescence microscopy (LSFM). This configuration avoids some problems such as the need of histological sectioning of the sample or low tissue penetration of light and the out-of-focus fluorescence that happens for the case of epi-fluorescence microscopy, while being able to acquire high-resolution images through a thick specimen at different axial depths. Good optical sectioning allows a straightforward tri-dimensional reconstruction of 2D images into a volumetric data set.

1.4.1. Selective Plane Illumination Microscopy (SPIM)

Light sheet fluorescence microscopy (LSFM) is a fluorescence microscopy technique with an intermediate optical resolution, but good optical sectioning capabilities and high speed. A laser light-sheet, which is focused only in one direction with the help of a cylindrical lens, is used for illumination. Thus, only a very thin slice of the volume is excited detecting the radiation to fluorescence on that specific slice. LSFM was developed in 1994 as orthogonal plane fluorescence optical sectioning microscopy or tomography (OPFOS) mainly for large samples and later as the selective plane illumination microscopy (SPIM) also with sub-cellular resolution which is the one used in this project.

Selective Plane Illumination Microscope uses one light sheet and one objective lens perpendicular to each other. The sample is placed at the focal plane at the intersection of the perpendicular paths of illumination and detection (Figure 6). The sample is moved in a stepwise manner along the axial direction to acquire parallel planar images

through the whole sample volume. Micrometric precision is achieved by means of a motorized stage that moves the specimen. CCDs or CMOS cameras are used to capture the images and allow fast acquisition of high quality images

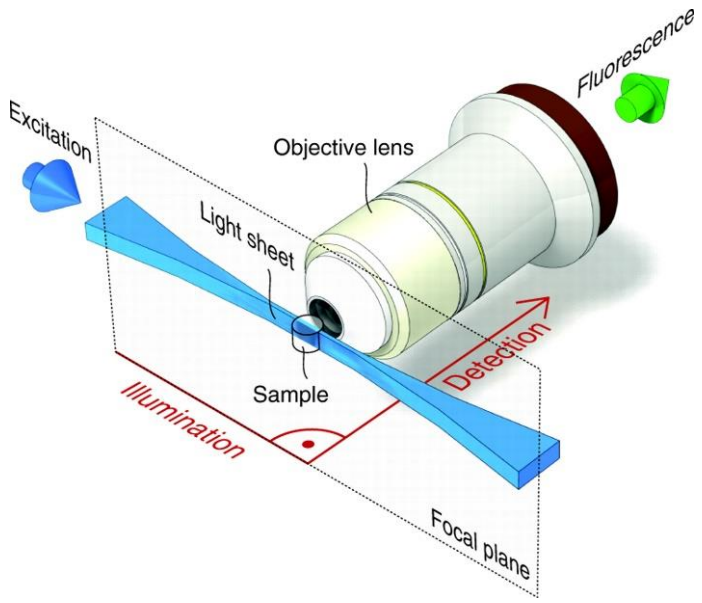

Figure 6. SPIM fluorescence microscopy setup. The light sheet illumination (blue) and the objective detection (green) perpendicular to each other with the sample in the focal pane of intersection *(from [13])*

The planar light sheet is obtained by the excitation laser going through a set of mirrors reaching the cylindrical lens. The dimensions of the light sheet can be adapted to different sample sizes: for small samples we can use a very thin sheet while for larger samples a thicker sheet is used. The thickness of the sheet is thereby related to the axial resolution of the data set. The shape of the beam is also far from ideally planar, presenting a Gaussian shape. We can observe in Figure 6 how the shape of the beam is broader at the ends and narrower towards the center. By placing the narrowest part of the light sheet in the center of the field of view, the sample will be illuminated with the most uniform part of it.

Fluorescence microscopy has some limitations such as photobleaching and photoxicity of the sample. Photobleaching occurs as the fluorescent molecules accumulate chemical damage from the electrons excited during fluorescence. Photobleaching can

severely limit the time over which a sample can be observed by fluorescent microscopy. Phototoxicity is produced by the molecular changes due to the absorption of light that causes toxiciy. Both effects are reduced with the Selective Plane Illumination configuration since excitation radiation is received only by the sheet-like volume that is illuminated at each time. In comparison with other fluorescence microscopy modalities in which the whole sample is excited during the entire time span of the scanning, the reduction in photobleaching can reach up to several orders of magnitude.

Selective Plane Illumination Microscopes are also limited by the scattering and absorption of light as it penetrates through the tissue leading the loss in resolution. This is due the optical absorption and scattering properties of the tissues that impede the excitation of the fluorophores. In order to minimize this absorption and scattering and thus compensate for this limitation, samples under study need to either be sufficiently thin or to present a high degree of transparency. There are some clearing protocols to achieve the transparency of the tissue that involved the incubation of the tissue in different solutions and at different temperatures during some days.

It is during this protocols when the sample is genetically modified such that fluorescent proteins label individual cells, particular tissues or whole structure in a process called immunofluorescence. Immunofluorescence is an antibody-based method to target fluorescent dyes to specific biomolecule targets within a cell, and therefore allowing the visualization of the distribution of the target molecule through the sample. Such fluorescent transgenic organisms offer the opportunity to visualize the cells and tissues with high resolution.

Depending of the fluorophore markers used in our sample different lasers with different wavelengths are used. Furthermore, multiple channels are available and can be acquired sequentially by simply changing the excitation laser light wavelength and the emission filter.

The reconstruction of the volume is achieved with the stack of high-quality two dimensional images from the data set acquired. Thus we can easily obtained 3D-images of organisms and multicellular samples in a faster manner.

1.4.2. Tissue clearing methods

When observing tissues under the Selective Plane Illumination Microscopy we encounter some disadvantages that reduce the resolution of the obtained image. The most important one is the absorption and scattering of light in tissues that avoid the excitation of the fluorophores and that increases as we go deeper in the tissue. Many clearing techniques have been developed in the last years to make tissues transparent and avoid this problem.

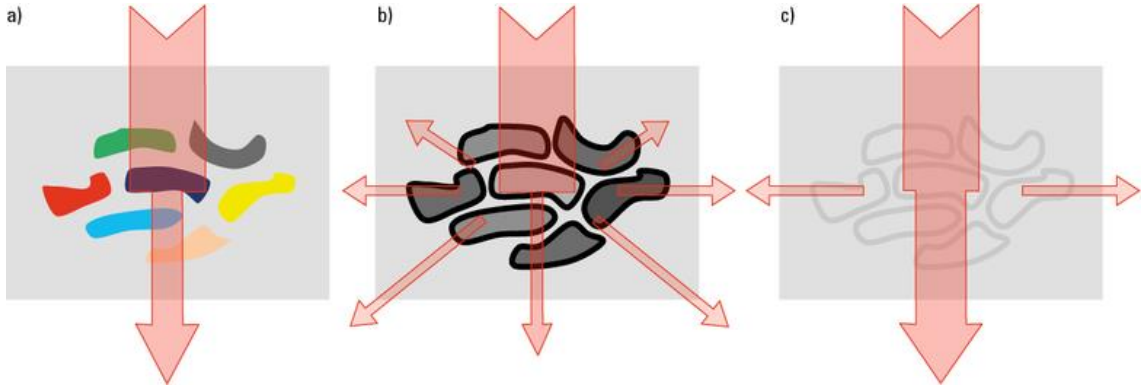

Figure 7. a) Low transparency through absorbing pigments; b) Low transparency due to effective scattering at surfaces with changing refractive index; c) High transparency after equalization of refractive indices *(from [14])*

Absorption of light occurs when the radiation (light) passes through a material (tissue) ongoing to its interaction and reducing the intensity of the light transmitted that is transformed into heat inside the tissue (Figure 7.a) . This happens due to the chromophores of the tissue, the part of the molecule responsible for its color, that absorb the light exciting and electron from it is ground state to an excited state. The amount of absorption of each chromophore depends on the tissue and on the wavelength used so clearing methods efficiently decolorized this chromophores present in the tissue [14].

The main problem is scattering that occurs at the many boundaries of changing refractive index due to different tissues (Figure 7.b). Clearing methods is equalize this

refractive index between tissues but without destroying the 3D structure preserving tissue organization at cellular and systemic level, and without degrading the possibly present fluorophores.

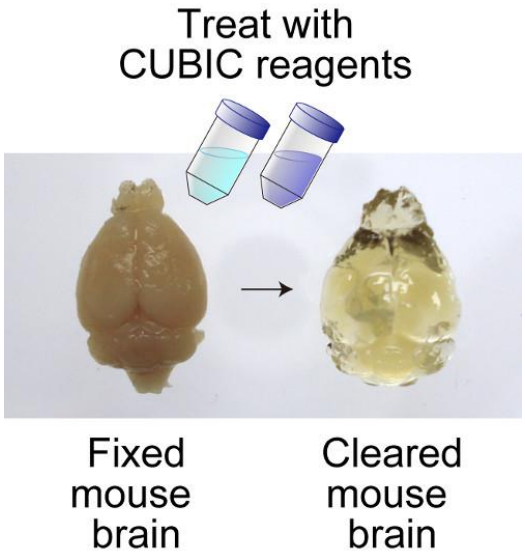

Figure 8. A mouse brain before (left) and after (right) clearing with amino alcohols using CUBIC clearing protocol *(from [15])*

Clearing methods combine chemical reagents to make the tissue transparent so that light passes through the tissue without losing intensity or suffering scattering (Figure 7.c), but many cases the lifespan of the present fluorophores obtained by immunofluorescence is reduced. There are some methods developed recently to preserve this fluorescence while achieving a high degree of transparency as the CUBIC (Clear Unobstructed Brain Imaging Cocktails) clearing method used in this project due to its simplicity and compatibility with SPIM microscopy. Another advantage of this method is the short required incubation period to make the tissue transparent since in other methods the incubation period could last weeks or months.

2. OBJECTIVES

2.1. Development of a high resolution fiber-optic fluorescence endoscope

Many biological and clinical studies require the analysis of morphology and function with cellular level resolution. The main objective of this project is the development of a fluorescence fiber-optic endoscopy system with a high resolution and quality imaging needed to examine the cellular level of any tissue. The difference of this endoscope with the traditional fiber-optic endoscope is that it uses only one fiber bundle (Figure 5.A) as insertion tube while the traditional one uses two or three fiber bundles (Figure 4) apart from other tubes and cables.

The purpose of this project is to test the fluorescence fiber-optic endoscopy system with two different optical fiber bundles: a fiber bundle in which the tip is directly in contact with the tissue and a fiber bundle with a GRIN (gradient-index) lens attached at the tip so that the tissue is located at a distance from the GRIN lens. With a LabVIEW program, real-times images captured with the fiber-optic endoscope can be viewed as well as videos can be recorded and saved for further analysis.

2.1.1. In-vivo application

During the in-vivo test, the fluorescence fiber-optic endoscope was tested on living mice under sedation and with a previously fluorophore introduced inside the intestine, in order to determine which configuration is optimal for imaging the colon.

The purpose is to use mice under induced cancer treatment so that they present some tumors in the colon that could be detected with our endoscopy system as well as test it in healthy mice. The fiber bundle of our endoscope was introduced in the colon of

the mouse through the anus and real-time videos showed us the intestinal tissue of the animal and allowed us to drive the fiber bundle inside the mouse intestine.

In-vivo experiments were performed at the Centro de Biología Molecular Severo Ochoa in Madrid in collaboration with Alicia Arranz, a postdoctoral researcher.

2.1.2. In vitro and microscopy validation

In-vitro tests in previously extracted fixed mouse colons were performed in order to validate the images obtained during the in-vivo test. This also allowed us to determine if the images obtained during in-vivo tests were actually a good determination for cancer diagnosis.

In-vitro experiments were also carried out at the Centro de Biología Molecular Severo Ochoa in Madrid in collaboration with Alicia Arranz.

A second validation of the results obtained with the fiber-optic endoscopy in-vivo and in-vitro was performed by using the SPIM. The same intestine tested in-vivo was cut into two fragments, tumor-free and tumor-bearing fragments, and was treated with immunofluorescence and with the CUBIC protocol for further analysis under SPIM.

The SPIM tests were performed at the Medical Imaging Laboratory at Hospital Gregorio Marañon in Madrid in a custom-made SPIM microscope mounted by Dr. Ripoll. The device includes five different excitation lasers of varying wavelengths and an assortment of emission filters (Table 3), which makes possible the use of more than one fluorophore per sample allowing the visualization of different cellular types.

3. MATERIALS AND METHODS

3.1. Fiber-optic endoscope components and system assembly

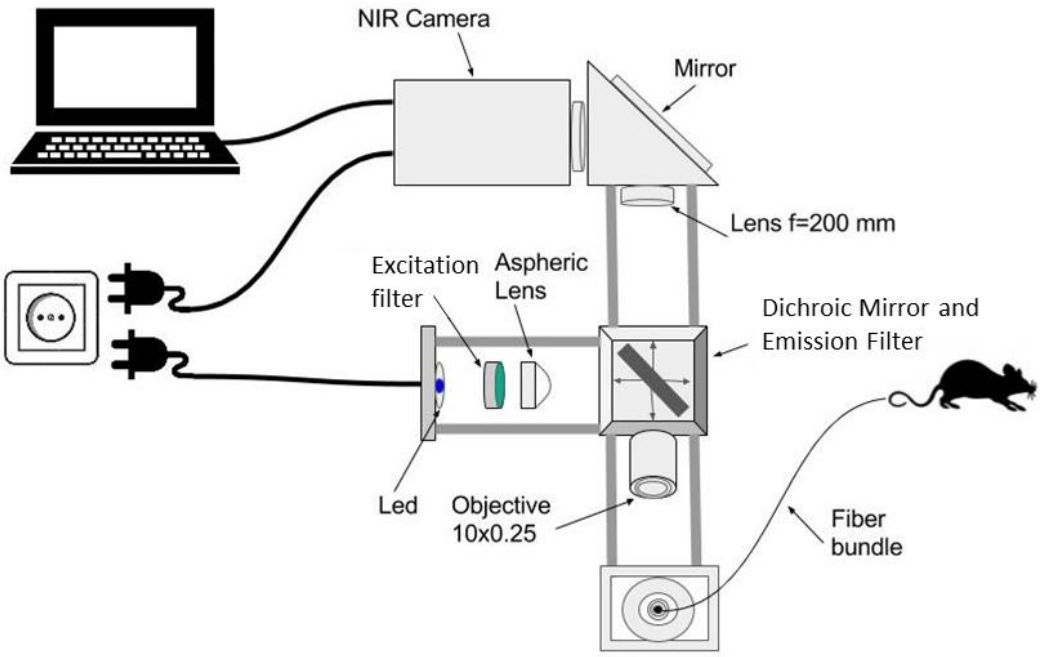

Figure 9. Scheme of the fiber-optic endoscope system

3.1.1. Near-Infrared Fluorescence camera

Near-infrared (NIR) fluorescence imaging techniques have been developed for a number of clinical applications, ranging from improving tumor delineation, lymph node identification,metastasis staging, to neuronal activity monitoring in the recent years. It is a very promising technique for image guided surgery since fluorescence imaging can

provide high sensitive and real-time information. NIR camera capture videos with and without excited fluorescence under the normal surgical room lighting condition in real time [16]. This particular camera is sensitive both to the visible and NIR wavelengths, thus expanding the range of fluorophores that may be used in our endoscope.

3.1.2. Illumination system

A light-emitting diode (LED), LED Ultraviolet 405 nm [25], was used as the light source of our system. A LED releases energy in form of light in an effect called electroluminescence. Electroluminescence is an optical and electrical phenomenon in which a material emits light in response to the passage of an electric current or to a strong electric field. It is the result of radiative recombination of electrons and holes in the semiconductor.

A LED is often in small area and we need extra optical components to shape its radiation pattern. An aspheric lens in needed to focus the LED radiation and an excitation filter, in this case, a band-pass filter is needed to limit the range of wavelengths that reach the dichroic mirror. The light is directed from the dichroic mirror through the optical fiber bundle reaching the sample and exciting their fluorophores.

Figure 10. LED used in the endoscopy system.

A laser that emits light coherently, focus on a spot and stay narrow over great distances (collimation), was also tested. In this particular case the illumination was

more homogeneous and more power is delivered with the LED so that we finally decided to use the LED as light source of our system.

3.1.3. Lenses and objective

Two different lenses and one objective have been used: a biconvex lens with focal distance 200mm, an aspheric lens, and one objective to adjust the light and focus the images.

3.1.3.1. Objective

The objective used has a magnification 10x, a numeric aperture of 0.25 that determines the light entering the objective and a working distance of 10.6 mm (Figure 11). The objective is composed of different lenses for which light penetrates and captures the image allowing us to obtain the maximum focused image and maintain a constant collimation.

Figure 11. 10X Olympus Plan Achromat Objective, 0.25 NA, 10.6 mm WD *(from [19])*

3.1.3.2. Biconvex lens

The biconvex lens with a focal distance f=200mm is placed before the NIR camera to focus the image of the fiber, captured by the objective, onto the camera. We adjust the distance of the fiber bundle so that we acquire a focused image with the NIR

camera. Depending on the fiber bundle (with and without GRIN lens) we have to move the coupling at which fiber is connected closer or further away from the objective.

3.1.3.3. *Aspheric lens*

An aspheric lens (Figure 12.A) is used to collimate the light coming from the LED. The term asphere encompasses anything that is not a portion of a sphere, however when we use the term here we are specifically talking about the subset of aspheres that are rotationally symmetric optics with a radius of curvature that varies radially from the center of the lens (Figure 12.B). Aspheric lenses improve image quality, reduce the number of required elements, and lower costs in optical designs [17] . The aspheric lens is placed between the band-pass filter and the dichroic mirror.

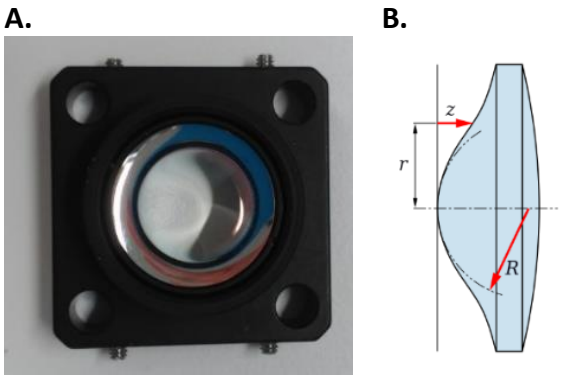

Figure 12. Aspheric lens. A. Aspheric lens used for our system assembly and B. Sketch of aspheric lens *(from [18])*

3.1.4. Filters and dichroic mirror

An emission filter and an excitation filter as well as a dichroic mirror are needed to filter the desired wavelengths and to redirect light to the direction we want. The excitation light coming from the LED passes through the excitation filter and is directed to the dichroic mirror. The dichroic mirror reflects the light through the objective towards our sample that is excited and re-emits light. This emission light is of lower wavelength and passes back through the objective to the dichroic mirror that transmits

the light as long as it is in a wavelength range. If any excitation light is able to pass through the dichroic mirror it will be blocked when it reaches the emission filter [20]. Light passing through the emission filter is then be focused onto the camera (Figure 13.A).

3.1.4.1. *Excitation filter*

The LED emits light in a rather broad wavelength range so that an excitation filter is needed to limit the wavelengths into a smaller range.

The excitation filter is a band-pass filter that is placed between the LED and the aspheric lens and has a central wavelength of 400 nm and a half-bandwidth of 40 nm and only transmits light that is able to excite the sample marked with the specific fluorophore. Only wavelengths between 360 nm and 440 nm are transmitted, whereas light with a greater or smaller wavelength will be blocked, to the dichroic mirror that redirect this light with this certain wavelengths so that they excite our sample. The choice of excitation filter and LED may be changed depending on the fluorophore being imaged.

3.1.4.2. *Dichroic mirror and emission filter*

The dichroic mirror and emission filter, separate different wavelengths so that they allow light of a certain wavelength to pass through, the one we are interested in (corresponding to fluorescence), while light of other wavelengths is reflected. The emission filter is a band-pass filter with central wavelength of 483 nm and a half-bandwidth of 31 nm. The dichroic mirror and the emission filter are plugged in together in a filter cube.

The dichroic mirror reflects the light coming from the source that has previously passed through the excitation filter (band-pass filter) to 45º to the sample and the emission filter only allows certain wavelengths coming from the sample to pass. The dichroic mirror has the following characteristic shown in Table 1.

Cut-On Wavelength (nm)	458	Wavelength at which the transmission increases to 50% throughput in a long pass filter.
Reflection Wavelength (nm)	415-450	Wavelengths directed to our sample from the LED source.
Transmission Wavelength (nm)	467-600	Wavelengths from our sample to the camera detection.
Dimensions (mm)	25.2 x 35.6	
Reflection (%)	98	
Transmission (%)	90	
Angle of Incidence (º)	45.0	

Table 1. Dichroic mirror specifications *(from [21])*

We want our sample to be marked with fluorophores with an excitation wavelength in a range of 415-450 nm and emission wavelength in a range of 467-600 nm. The fluorophore used is this project was Acriflavine that is an acridine, an organic compound and a nitrogen heterocycle with the formula C13H9N, that we dissolved in water at a concentration of 0.01%. Acriflavine has an excitation wavelength of 460 nm and an emission wavelength of 514 nm in water (Figure 13.B).

A.

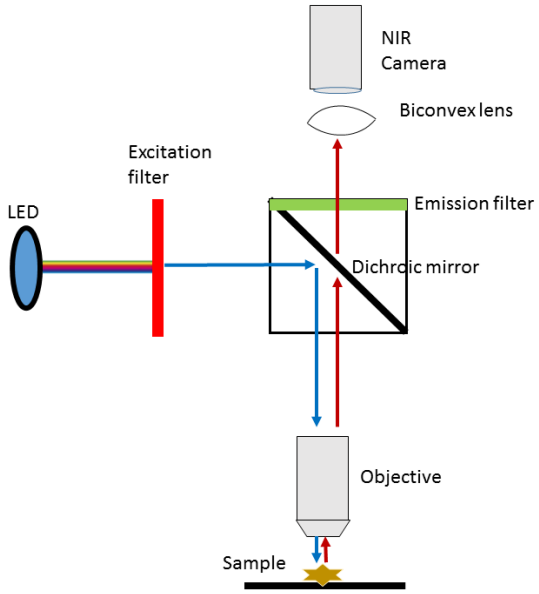

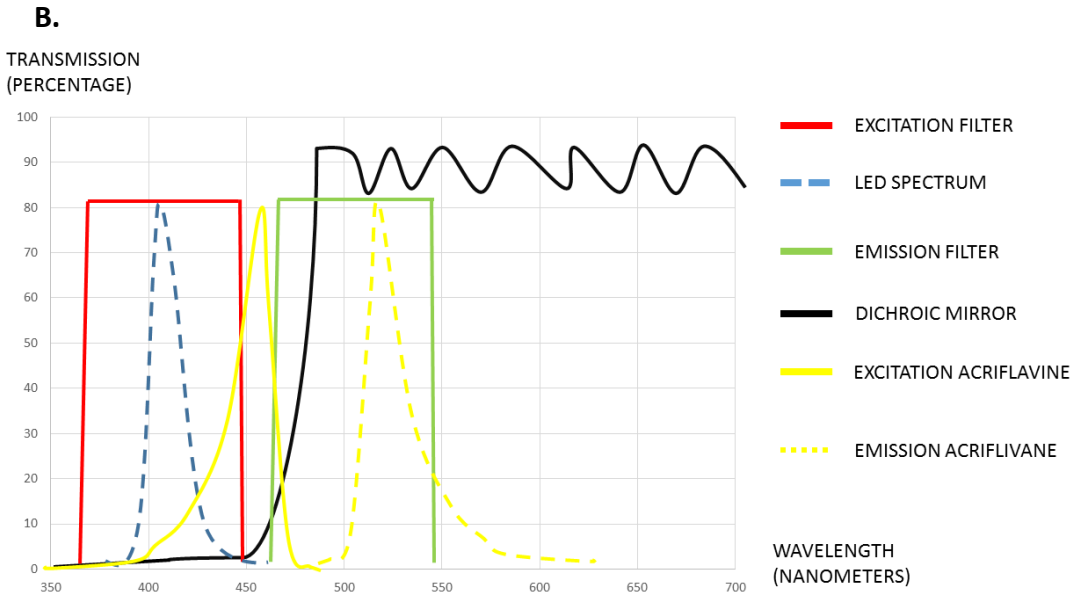

Figure 13. A) Light path through excitation/emission filters and dichroic mirror B) Spectrum of the Fluorescence Filter Combination and Acriflavine.

3.1.5. Optical fiber bundle

A fiber bundle is a cable containing many optical fibers that are used to carry light. The optical fiber elements are typically individually coated with plastic layers and contained in a protective tube. The optic fibers used in this project are Fijikura image fibers. Fujikura is one of the world's leading manufacturer of fused silica-based coherent image fibers [22]. They have excellent image carrying characteristics and they are suitable for use in both medical and industrial applications.

We have chosen FIGH series N-type since they are extremely thin providing great image quality with very high-resolution in ultra-thin diameters, high pixel density as well as great contrast and color with no defects. Also, they have high durability, flexibility and affordable pricing. Therefore, this kind of fibers are ideal for endoscopes due to its small size providing vision to previously inaccessible locations. The fiber chosen for this project has 30.000 fibers and it has an outer dimeter of 1 mm. Each individual fiber has a diameter of 5 µm.

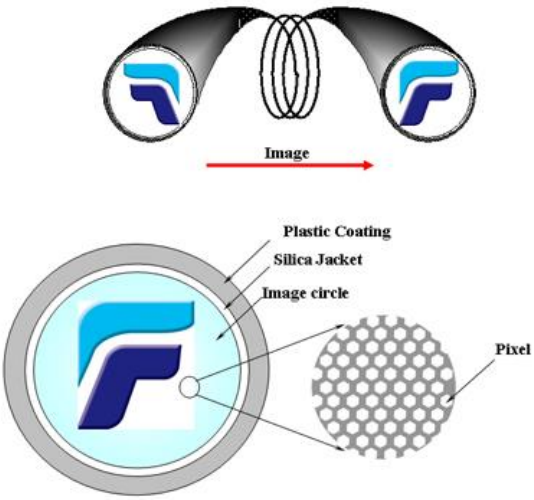

Figure 14. Fijikura image fiber cross section structure *(from [23])*

In order to assemble the fiber to our system we attached a 4'w/ SMA (SubMiniature version A) connector at the end of the fiber bundle (Figure 15.A) with a special glue. The aperture of the SMA connector should be a little bit large than the diameter of the fiber bundle so this can pass through it. Once the fiber and the SMA connector are assembled (Figure 15.B) we can connect the fiber to the fiber bundle coupling located in front of the box of our system (Figure 20) so that it is ready to be used.

A.

B.

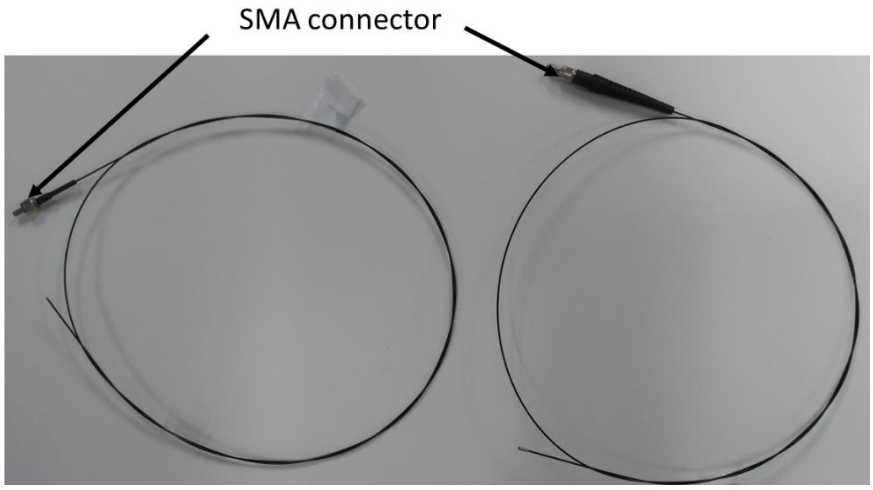

Figure 15. A) SMA connector B) Fiber bundles with (left) and without (right) GRIN lens and SMA connector assembly

3.1.5.1. GRIN lens

Gradient-index (GRIN) optics is the branch of optics covering optical effects produced by a gradual variation of the refractive index of a material. Such variations can be used to produce lenses with flat surfaces, or lenses that do not have the aberrations typical of traditional spherical lenses. Gradient-index lenses may have a refraction gradient that is spherical, axial, or radial.

The spatial resolution of the endoscope can be increased by attaching a GRIN lens, which is compatible with fiber-optics, to the distal tip of the fiber bundle. These optics are configured such that instead of placing the bundle tip directly on to the tissue, the tip is imaged onto the tissue surface, thereby increasing the spatial sampling frequency imposed by the light-guiding cores of the fiber bundle.

In our case we assemble a GRIN lens to the distal tip of a fiber bundle (same fiber as the previous one). The GRIN lens was obtained from GrinTech and with the following characteristics: working distance 1mm, fields of view 55º, depth of field 1,5mm. In the GRIN lens the light rays are continuously bent within the lens until they are finally focused on a spot (Figure 16).

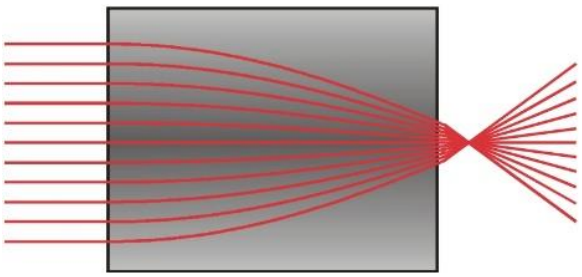

Figure 16. Rays path through GRIN lens *(from [24])*

Appropriately choosing the lens length causes the image plane to lie directly on the surface plane of the lens so that sources such as optical fibers can be glued directly onto the lens surface (Figure 17). The diameter of the GRIN lens must exceed that of the fiber bundle so that all cores of the fiber bundle are fixed to the GRIN lens. In this case we ordered a fiber with the GRIN lens already stuck to it.

During this project we are going to test two different fiber bundles, one nude fiber bundle without anything at the tip and one fiber bundle with a GRIN lens attached to it. The advantage of the fiber bundle with the GRIN lens is that the tip has not to be in direct contact with the tissue we are exploring as it happens with the nude fiber bundle. The fiber with the GRIN lens has also a higher field-of-view is higher. On the other hand the nude fiber bundle has higher resolution than the fiber bundle with the GRIN lens attached to it.

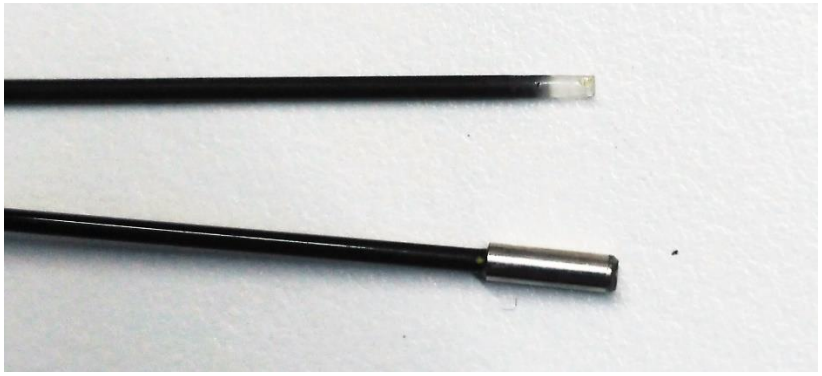

Figure 17. Fiber bundle without (upper) and with (down) GRIN lens.

3.1.6. Final system assembly

All the system is placed inside a box designed for it. The box has an exit for the power supply, an exit for the computer connection, a power button to turn on and off the LED and an exit for the fiber bundle connection and focusing system. This box will allow to displace the whole system to any laboratory in which we want to use the endoscope, and will allow doctors or researchers to use the fluorescence fiber-optic endoscope in an easy and achievable way.

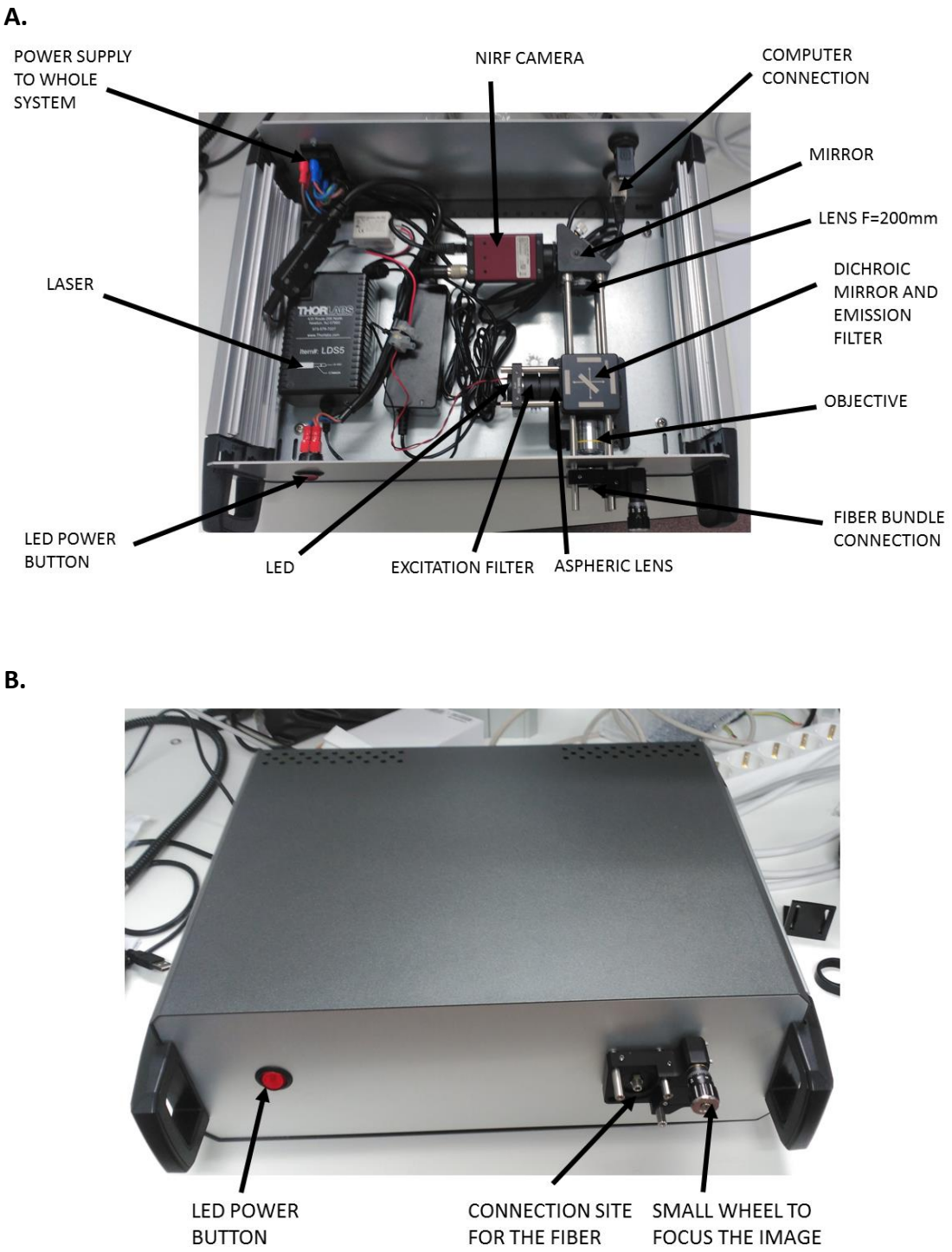

Figure 18. Fiber bundle endoscope A) Open box with all components and B) Close box.

3.2. Fiber-optic endoscope control with LabVIEW program

A LabVIEW program of National Instruments is used to control our endoscope system and allows us to acquire real-time images. National Instruments is a unique platform which approach is the engineering and science applications that has driven progress across a wide variety of industries. Central to this approach we have LabVIEW, a development environment designed specifically to accelerate the productivity of engineers and scientists. LabVIEW has graphical programming syntax that makes it simple to visualize, create, and code engineering systems helping engineers translate their ideas into reality, reducing test times, and delivering business insights based on collected data. It helps to solve problems faster and more effectively saving money and improving product quality [26].

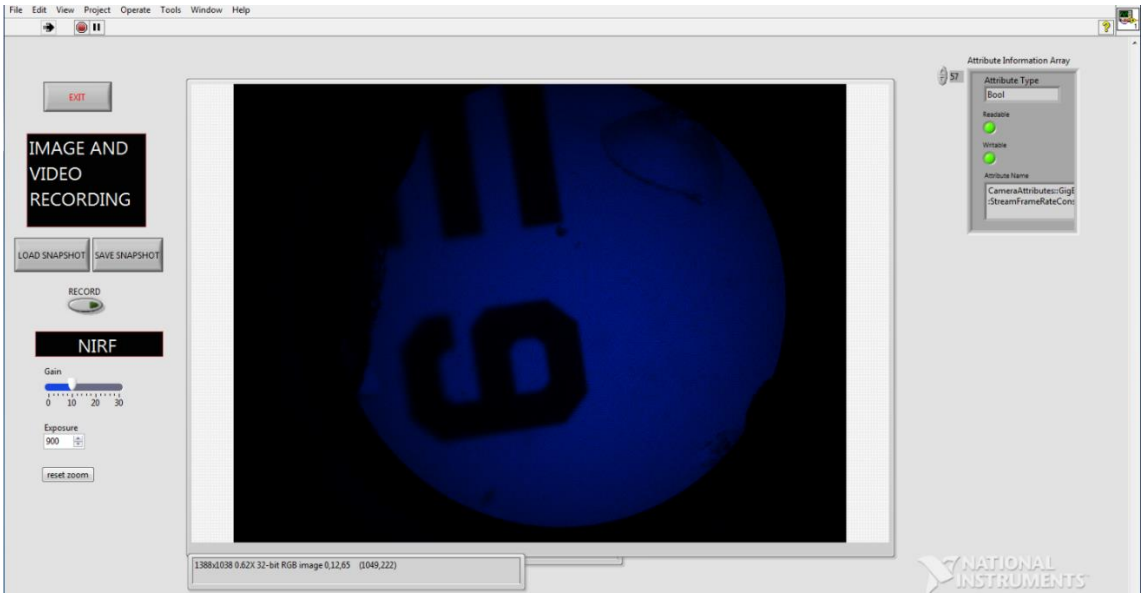

Figure 19. Interface of the fiber-optic endoscope LabVIEW program.

IMAQ Vision library of LabVIEW was used for the NIR camera detection and to develop the imaging applications needed for the image acquisition [27]. In order to record a video we have to press RECORD button so that a video starts to save in a folder in .avi format on our computer. We are also able to save a single image in .tiff format with

the button SAVE SNAPSHOT and to return to the default zoom with RESET ZOOM. Finally we can control the signal to noise ratio of the image with the bar GAIN and the changing values box EXPOSURE.

3.3. Calibration protocol

The calibration protocol establishes how to properly use the fiber-optic endoscope system obtaining the desired results and without any chance to break the system. The steps of the calibration protocol are the following:

1. Connect the fiber-optic endoscope box (from behind) to the power supply with a power cord.
2. Connect the fiber-optic endoscope box (from behind) to the computer with an Ethernet cable.
3. Assemble the desired fiber-optic (with our without GRIN lens) to the fiber-optic coupling of the endoscope box.

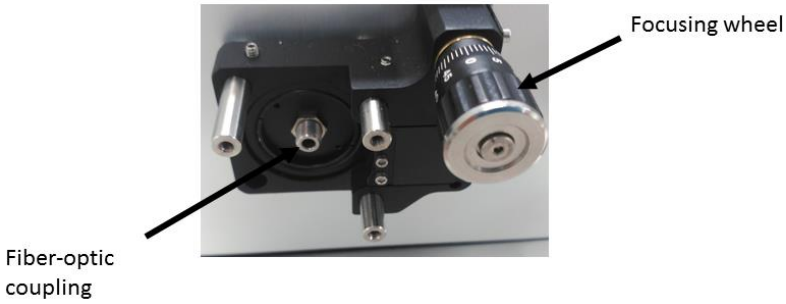

Figure 20. Fiber–optic coupling where the fiber is threaded and the focusing wheel to focus the image.

4. Turn on the power supply of the endoscope box with the power button located in the front part of the endoscope box.

5. Turn on the LED power supply with the power button located in the front part of the endoscope box. Once this step is done, the laser light should be seen at the end of our optical fiber already connected.
6. Open the LabVIEW program in the computer and run the program.
7. Point the fiber bundle at the lights so that you are able to see a homogeneous image.
8. Focus the image with the small wheel located in the fiber-optic coupling in the front part of the box as we can see in (Figure 20). This small wheel moves the fiber-optic coupling in very little distances so that we can perfectly obtain a focused image in which we can easily see the individual cores (Figure 21.C).

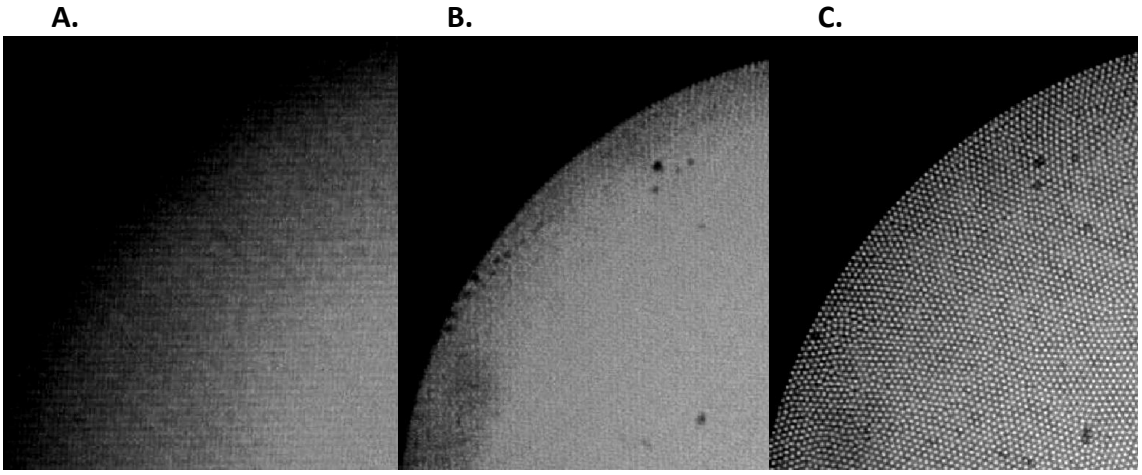

Figure 21. Examples of imaging with the fiber-optic bundle. A) Poor focus B) Good focus C) Ideal Focus

9. Improve quality of the image with the bar GAIN and the changing values box EXPOSURE of the LabVIEW program and save images or record videos with SAVE and RECORD buttons respectively.
10. Clean the fiber bundle with isopropanol to remove dust before and after each use.

3.4. Resolution

In order to characterize our fibers, we have to establish the resolution of the one without GRIN lens and the GRIN lens fibers. In order to determine the resolutions we used a 1'' USAF-1951 Test Target (Figure 22.A) that is widely accepted to test the resolution of optical imaging systems such as microscopes, cameras and image scanners. These targets have 6 groups (+2 to +7) with 6 elements of horizontal and vertical lines, offering a maximum resolution of 228.0 line pairs per millimeter which equates to roughly 4.4 µm per line pair [28]. The largest set of non-distinguishable horizontal and vertical lines (Figure 22.B) determines the resolving power of the imaging system. Table in Figure 23 indicates the lines pairs per mm (lp/mm) for a given element of a group based on the equation below, where the line pair (lp) means a black and a white line.

$$Resolution\left(\frac{line\ pair}{mm}\right) = 2^{Group+\left(\frac{Element-1}{6}\right)}$$

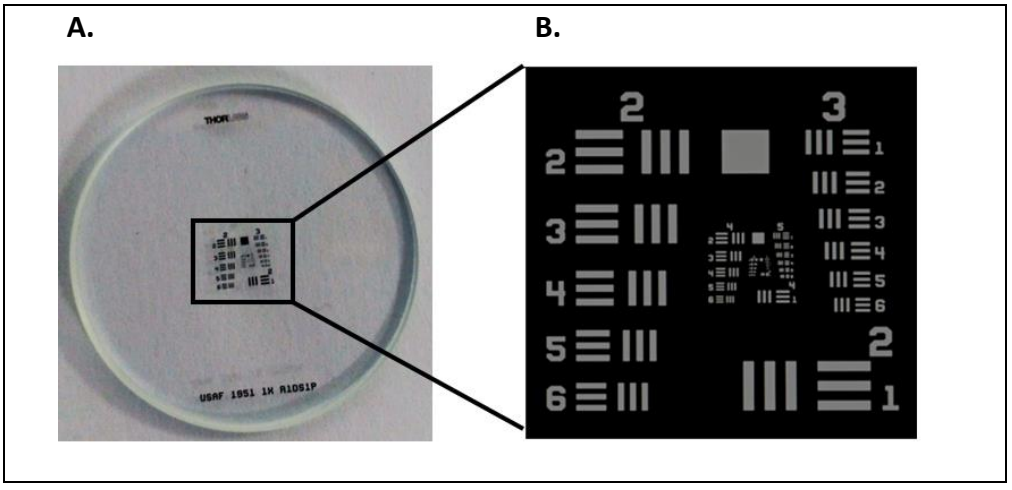

Figure 22. A) USAF Test Target B) Set of group lines and numbers that determine the resolution *(from [28])*

Element	Group Number									
	-2	-1	0	1	2	3	4	5	6	7
1	0.250	0.500	1.00	2.00	4.00	8.00	16.00	32.00	64.00	128.00
2	0.280	0.561	1.12	2.24	4.49	8.98	17.95	36.0	71.8	144.0
3	0.315	0.630	1.26	2.52	5.04	10.10	20.16	40.3	80.6	161.0
4	0.353	0.707	1.41	2.83	5.66	11.30	22.62	45.3	90.5	181.0
5	0.397	0.793	1.59	3.17	6.35	12.70	25.39	50.8	102.0	203.0
6	0.445	0.891	1.78	3.56	7.13	14.30	28.50	57.0	114.0	228.0

Values are in lp/mm.

Figure 23. Table of number of lines pairs/mm depending on the element and the group. *(from [28])*

Fiber without GRIN lens

In the case of the fiber without the GRIN lens the resolution was measured by placing the end of the fiber directly on top of the Test Target surface.

Fiber with GRIN lens

The resolution of the fiber-optic with the GRIN lens was measured by placing the Test Target onto a small translation motor (Zaber, Canada), which we were able to control from the PC. We first placed the fiber-optic on a foot with its GRIN lens surface in direct contact with the Test Target surface (Figure 24) and we started to move further away the Test Target in 0.02 cm increments.

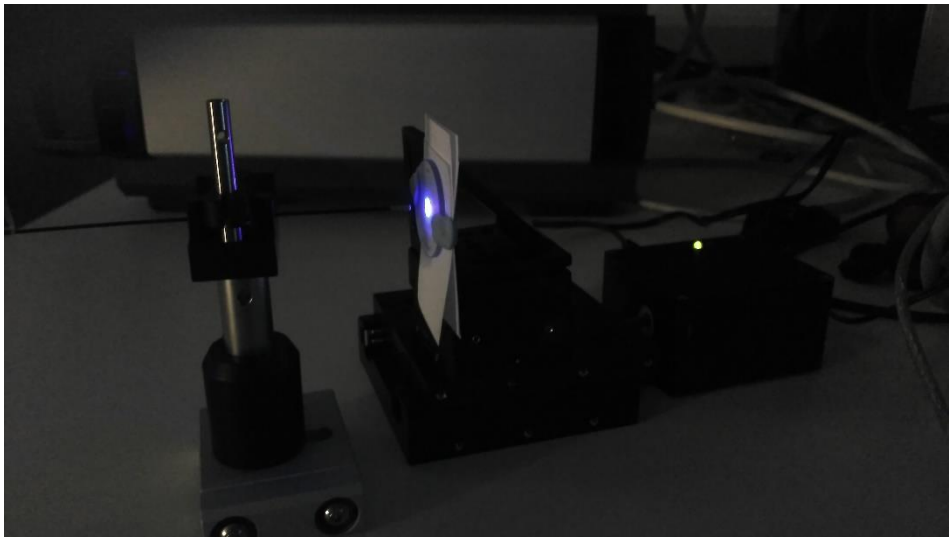

Figure 24. Fiber-optic with GRIN lens placed on a foot and Test Target on the small engine.

3.5. In-vivo test

Several experimental models of colon carcinoma have been developed to provide a better understanding of the disease in humans. The analysis of these models have provided evidence of the correlation between a chronic inflammatory status in the colon and the development of cancer.

In this project, AOM/DSS mouse model [29] is used to induce colorectal cancer. In this model, the administration of azoxymethane (AOM), a typical compound use in biological research for the induction of cancer by favoring the introduction of mutation in DNA, is combined with the administration of the inflammatory agent dextran sodium sulphate (DSS), which induces an inflammation on the mouse colon that mimics the clinical and histological features of Inflammatory Bowel Diseases in humans, an inflammatory, chronic and autoimmune disorder that mainly affects the colon.

When colorectal cancer is induced abnormal tissue growths from the internal mucosa of the colon called polyps appears. Sometimes this polyps are benign but in many cases they derive in a carcinoma and the destruction of the tissue, leading to the disappearance of the crypt structure and producing aberrant crypt foci.

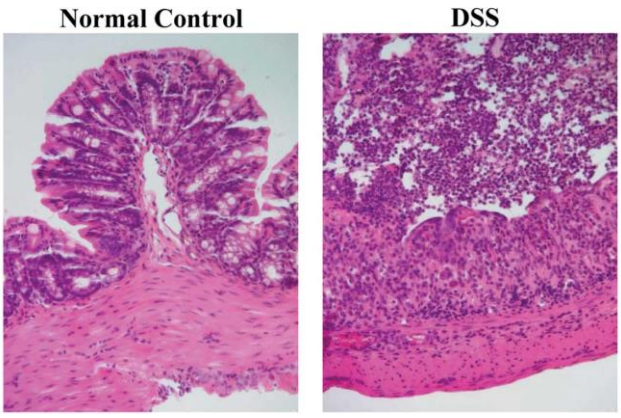

Figure 25. Normal control mice displayed normal colonic histology with an intact epithelium where crypts are well defined while in DSS we can observed that the epithelium has been destroyed and the crypt structure has disappeared *(from [30])*

The in vivo experiment provide us to detect the development of the tumor and metastasis without the extraction of the intestine of the mouse. We have performed several tests with the fiber-optic endoscope without the GRIN lens and with the GRIN lens fiber bundles. Acriflavine was used as fluorescence dye due its convenient excitation and emission wavelengths (Figure 12.B). The fluorescence is inserted in the mouse intestine topically, directly through the intestine cavity, avoiding thus the intravenously administration with a needle which is harder and more invasive.

The fiber is introduced in the colon of the mouse through the anus and with the LED turned on. The real time images are seen with the LabVIEW program and the gain and exposure times are changed as desired in order to improve the illumination of the image. Real-time video allowed us to easily drive the fiber bundle through the intestine of the mouse while simultaneously several videos were recorded during the experiment for further study.

Before and after each experiment, the fiber was cleaned with a lens cleaning tissue moistened in isopropanol (alcohol) being careful at the tip of the optical fibers. Lens cleaning tissues are special for glasses and mirrors to remove small particles.

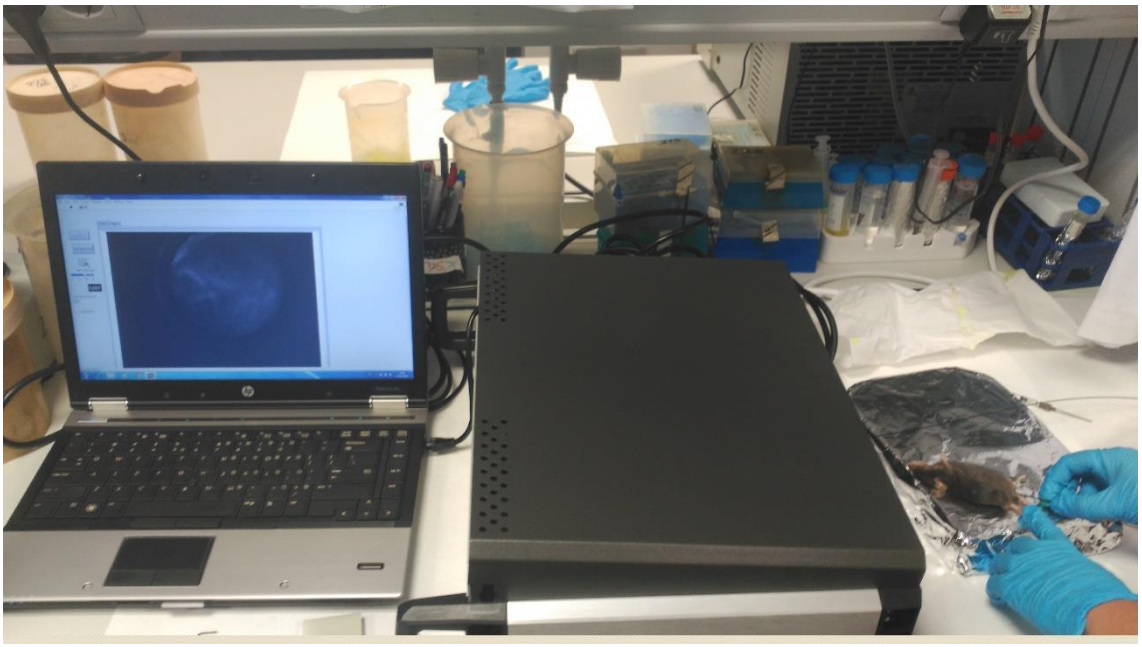

Figure 26. Testing the fluorescence fiber-optic endoscope in in-vivo (mouse) with the fiber bundle without GRIN lens.

Apart from the test on AOM/DSS mouse model other in-vivo tests in healthy mice were performed so we could reach to a more real conclusion of the results.

3.6. In-vitro test

The fluorescence fiber-optic endoscope is tested in previously extracted fixed colons of healthy mice to validate the images obtained during in-vivo tests. The procedure is the same as before: fluorescence is topically administered inside the intestine cavity with a needle, the fiber-bundle endoscope is then introduced in the cavity with the help of tweezers and real-time videos are recorded for further analysis.

A. **B.**

Figure 27. In-vitro test. A) Acriflavine at 0.01% of concentration (left) and fixed mouse intestines in PBS (right), and a petri dish (down) in which the experiment was performed B) Insertion of the optic fiber with the help of tweezers through the fixed mouse colon.

3.7. 3D image acquisition with SPIM microscope

Selective Plane Illumination Microscope was used in extracted colon of the AOM/DSS mouse model previously analyzed in-vivo. This colon was cut in different fragments so that we keep the interested ones: one fragment free of cancer and one fragment with a clearly tumor in it. This two fragments were cleared and then examined under SPIM.

3.7.1. CUBIC clearing protocol

CUBIC clearing protocol was used in this project to clear the interested tissues to properly image them under SPIM based on the Susaki et al. CUBIC protocol [31]. This protocol is based on both the removal of lipids, molecules that produce light scattering, and homogenization of the refractive index throughout the whole sample. The protocol implies the immersion of the sample into two reagents and the immunostaining of the sample. Reagent 1 allows lipid removal from our sample and Reagent 2 adjusts the refractive index through the whole brain. Immunostaining of the sample implies the target of fluorescent dyes to specific molecules in the sample. We used Alexa Fluor 647 Phalloidin, fluorescent probe used to visualize actin filaments under microscopy, and DAPI (4',6-diamidino-2-phenylindole), a fluorescent stain used to see cells of a tissue under microscopy.

3.7.1.1. Solutions

Reagent 1 (20 mL)

Add to a glass beaker 7 mL of distilled water, 5 g of urea and 5 g of N,N,N',N'-tetrakis(2-hydroxy-propyl)ethylenediamine. This chemical is highly viscous, so it can be used diluted at 80% in water. Dissolve the mixture by stirring. This solution doesn't need to be heated, although increasing the temperature for a short amount of time will help dissolve faster. If it was heated, when the temperature is back to room temperature add 3 mL of Triton 100x and mix by stirring.

Triton is a detergent whose function is to increase the permeability of the cell membrane facilitating the diffusion of the polyalcohol that will remove the lipid molecules. Urea is an organic compound that will increase the refractive index of the tissue, diminishing the light scattering properties.

Reagent 2 (40 mL)

Add to a glass beaker 6 mL of distilled water, 4 g of Triethanolamine (10 wt%) and 20 g of Sucrose. Let it dissolve on a heated stirrer. Increase the temperature to almost 100

ºC. Avoid overheat of the solution; it will dissolve in approximately 15 minutes. When it's almost dissolved, decrease the temperature but keep stirring. Add 10 g of urea and let it dissolve on non-heated stirrer in order to prevent decomposition of urea. Cool down the solution to room temperature and add 40 µL of Triton 100x (0.1%) and mix by stirring. Leave the reagent 4 days at rest so that possible bubbles produced during the process rise to the surface and disappear.

Sucrose 30% (30 mL)

Add 9 g of Sucrose in 30 mL of 1x PBS and mix by stirring on a stirrer or with a vortex.

Sucrose 50% (40 mL)

Add 20 g of Sucrose in 40 mL of 1x PBS and mix by stirring on a stirrer or with a vortex.

Fluorescent labeling Solutions

Add 0.1 g of Bovine Serum Albumin (BSA) to 20 mL of PBT 0.1% that is made up of 20 mL of PBS and 100 µL of Triton 100x (0.1%).

3.7.1.2. Protocol for mouse colon

DAY1

Each selected colon fragment was cleaned with tweezers in order to remove hairs and some fuzz carefully to do not damage it. Then, each fragment was submerged in 10 ml of degassed Reagent 1 in a 50 mL Falcon tube and left for 7 days at 37 ºC in an incubation shaker in slow motion. Reagent 1 of the tumor fragment was changed for new prepared Reagent 1 at day 3 while the fragment without colon was maintain in the same Reagent 1 solution for the 7 days. This solution change was done since the tumor fragment size was larger than the tumor-free fragment size so it would be more difficult to clear it.

DAY2

The samples were washed in clean 50 mL Falcon tubes with 1x PBS. Minimum 3 washes of 10 minutes were done in a shaker at room temperature.

15 µL of Alexa Fluor 647 Phalloidin, at concentration 1:100, and 0.3 µL of DAPI, at concentration 1:5000, were added to 1.5 mL of the fluorescent labeling solution. This is done twice, one for each sample.

Each sample was submerged on 1.5 mL of this solution and incubated in a rotor in motion at a refrigerator (4ºC) for 3 days.

DAY3

Samples were washed in PBT 0.1% in the same conditions as before in clean 50 mL Falcons and were submerged in 15 mL of 30% sucrose/PBS 1x each and incubated in a rotor in motion in a refrigerator (4ºC) for 1 day. Based on [32].

DAY4

Both fragments were submerged in 20 mL of 50% sucrose/PBS 1x each and incubated in a rotor in motion in a refrigerator (4ºC) for 3 days. Based on [32].

DAY5

Each colon fragment was submerged in 20 mL of Reagent 2 in a laboratory glass tube and incubated at 37 ºC in a shaker in slow motion for 1 or 2 days.

The samples can be then stored in a refrigerator (4ºC) until they are going to be imaged. Reagent 2 precipitates at low temperatures, so before imaging submersion in a water bath at 37 ºC until it becomes completely liquid and transparent is needed.

3.7.2. SPIM image acquisition

The SPIM system has an excitation laser that is directed through a set of mirrors towards a cylindrical lens that will create the light sheet. The illumination objective used to direct the laser sheet in the focal plane is an infinity corrected 5x long working distance objective (Mitutoyo; NA 0.14, WD 34 mm, DF 14 µm). For the detection, two infinity-corrected long working distance objectives (Mitutoyo) of different magnification were available (Table 2).

2x detection objective: numerical aperture (NA) 0.055, working distance (WD) 34 mm and depth of focus (DF) 91 µm.
5x detection objective: numerical aperture (NA) 0.42, working distance (WD) 34 mm and depth of focus (DF) 14 µm.

Table 2. Two different magnification objectives available in the setup of the SPIM microscope at Medical Imaging Laboratory, Hospital Gregorio Marañon.

The sample to be imaged was immersed in a cylindrical glass tube filled with Reagent 2. The cylindrical glass tube is positioned inside a custom-made glass cuvette (Hellma Analytics) filled with oil (Johnson Baby Oil, Johnson & Johnson) since it is a cost-effective solution that matched the high refractive index of glass or another component, depending on the experiment. The oil is used to match the RI of the sample under study and its immersion medium. A joystick with three degrees of freedom is also used to control the movement of the detection objective and the sample.

The imaging system consists of a scientific CMOS camera (Neo 5.5 sCMOS, Andor Corp) thermoelectrically cooled to reduce electronic noise. The sensor has 2560x2160 active pixels and the physical detector size is 6.5 µm x 6.5 µm. The final resolution of the image will depend on the magnification of the detection objective and on the binning used. Binning is the aggrupation of two or more sensor adjacent pixels in order to achieve faster readout speeds and improved signal to noise ratios.

The immunostained samples present data in two different channels, one for the DAPI nuclear counterstaining and one for Alexa Fluor 647 Phalloidin. To visualize the DAPI stained tissue, the sample was illuminated with the 405 nm laser and the emitted fluorescence signal was collected with a 475 nm emission filter. Alexa Fluor 647 fluorochrome required illumination with the 635 nm laser and signal collection with the 670 nm filter.

Excitation laser λ	Emission filter λ/bandwidth	Matching Spectra Fluorophores
405 nm	475/50 nm	DAPI dye
473 nm	531/40 nm	AlexaFluor 488, GFP
532 nm	607/70 nm	AlexaFluor 555, Cy3 dye
590 nm	700/40 nm	AlexaFluor 594, mCherry
635 nm	670/10 nm	AlexaFluor 647, Cy5 dye

Table 3. Excitation lasers and emission filters available in the setup of the SPIM microscope at Medical Imaging Laboratory, Hospital Gregorio Marañón. In the third column fluorescent labeling and dyes with matching excitation and emission spectra

The detection was performed using 2x and 5x magnification lenses (Table 2). The acquired 3D image data set is automatically assembled as a TIF composite stack of all the acquired channels.

3.8. Image processing

Images acquired with the fiber-optic endoscope and the SPIM microscope were processed with ImageJ Open Source software. This free software constitutes a powerful tool for biological image analysis. A huge number of filters and plugins are available and batch processing of a large set of images can be easily implemented through macro programming. For the case of SPIM microscope, the volumetric reconstruction of the image stack was performed with the ImageJ 3D project.

4. RESULTS AND DISCUSSION

With the fluorescence fiber-optic endoscope we were able to analyze the tissue structure of the mouse colon, detecting the characteristic crypt structure mentioned at the introduction. Several videos were recorded during in-vivo and in-vitro tests and 3D reconstructions were performed from the stacks of images obtained during SPIM measurements.

4.1. Optical fibers

With respect to the optical fibers we realized that the GRIN lens does not provide sharp images when dealing with true 3D geometries such as the colon so it was not appropriate for endoscopy. With this fiber we were not able to detect the crypt structure of the colon tissue obtaining poor results. We only obtained good results with the fiber bundle without the GRIN lens that are the ones shown in the results.

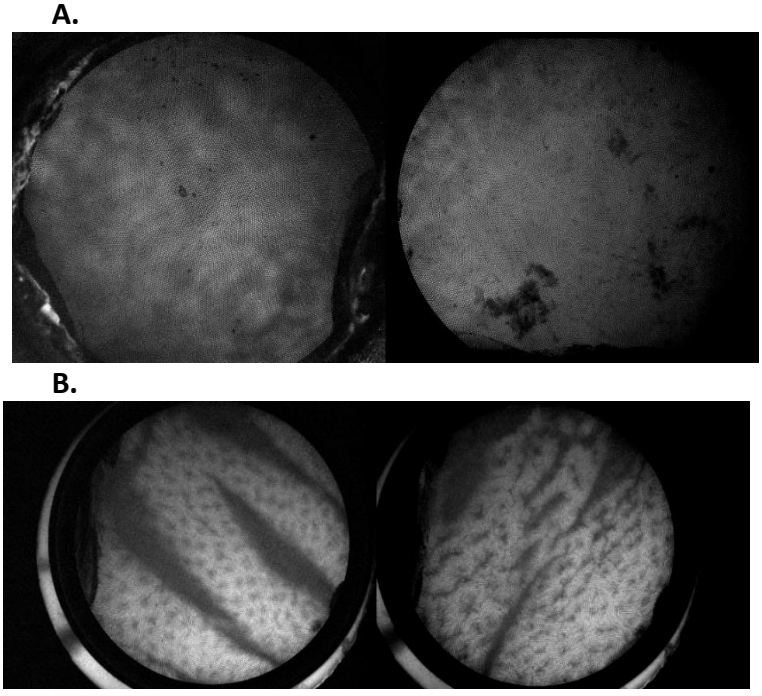

Figure 28. Colon of a mouse seen with the fiber-optic endoscope in-vitro A) with GRIN lens and B) without GRIN lens

4.1.1. Resolution

Fiber without GRIN lens

As we can see in (Figure 29) the largest set of non-distinguishable lines is element 3 of group 7, placing the resolution of the fiber-optic without GRIN lens is 161.0 lp/mm.

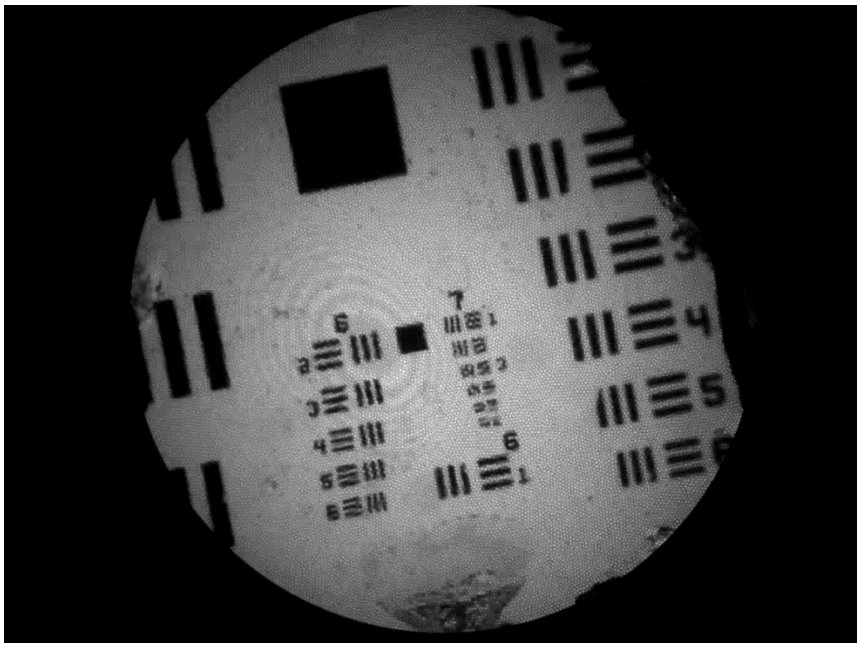

Figure 29. Picture of the smallest set of lines of the test target obtained with the fiber-optic without GRIN lens

Fiber with GRIN lens

Once all images were obtained in 0.02 cm increments the image with the best quality was at approximately 0.2cm as we see in (Figure 30). At that distance the largest element we were not able to distinguish was 4 of group 2, placing the resolution of the GRIN lens fiber-optic at 5.66 lp/mm.

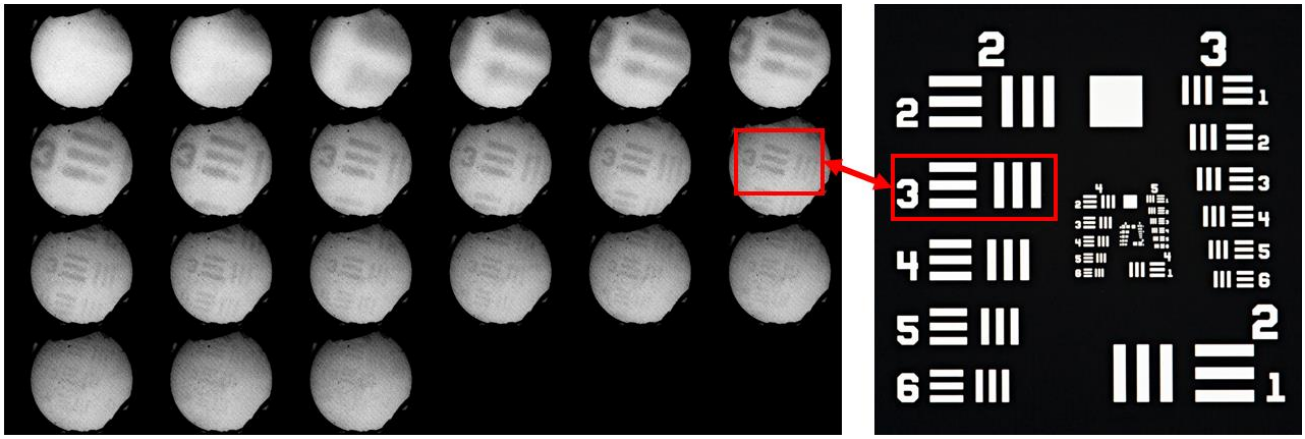

Figure 30. Images of element 4 and group 2 of the Test Target taken in 0.02 cm increments starting at distance 0 cm. GRIN lens surface in contact with Test Target surface (first image) and moving far away until 0.42 cm, distance from GRIN lens to Test Target (last image).

4.2. In-vivo results

The In-vivo results were performed on a healthy mice as well as on a mouse with induced cancer as mentioned before, AOM/DSS mouse model. In all cases Acriflavine was previously topically inserted in the mouse colon.

We realized during the in-vivo test on AOM/DSS mouse model that there were areas of the colon tissue where the crypt structure was easily detected (Figure 31.A) and that there were other areas where the tissue was destroyed and no crypt structure appeared (Figure 31.B). We reached to the conclusion that the difference was between tumor-free areas and a cancer affected areas.

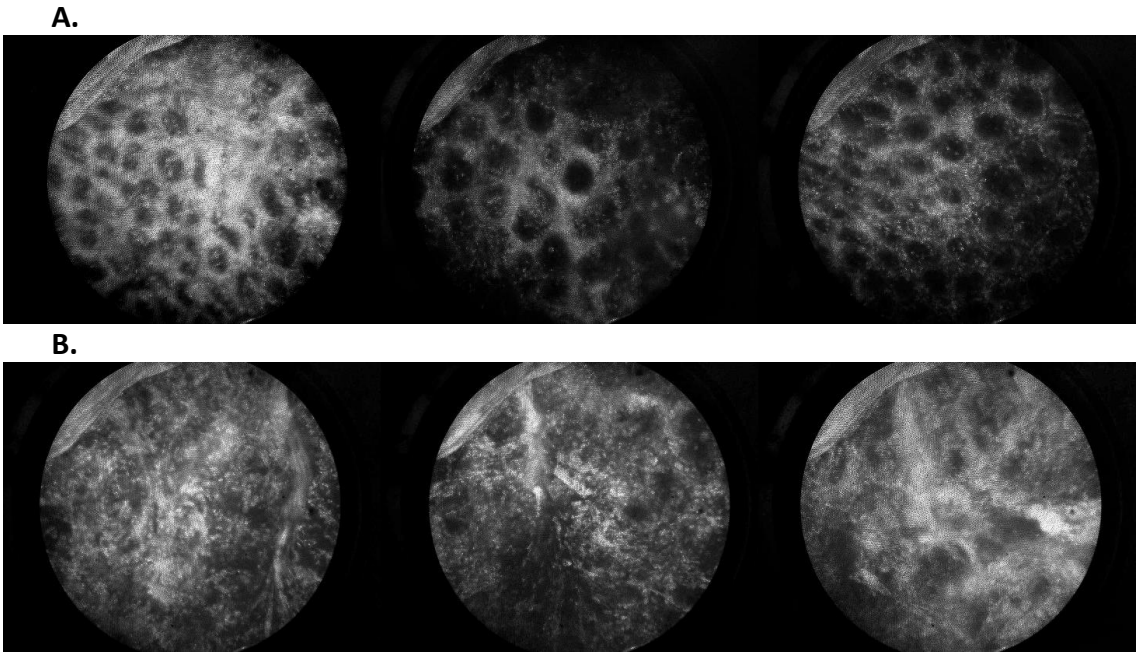

Figure 31. Colon of a mouse seen with the fiber-optic endoscope in-vivo. A) Tumor-free area in which we can appreciate the crypt structure of the intestine. B) Tumor affected area in which we can see how the crypt structure disappears.

There were also some parts of the tissue that were quite destroyed in a step between tumor-free tissue and tumor formation in which we detected some crypt that has been increased in size and with the tissue surrounding almost destroyed (Figure 31.B)

More in-vivo tests were performed in healthy mice in which we were able to detect the crypt structure on the whole colon.

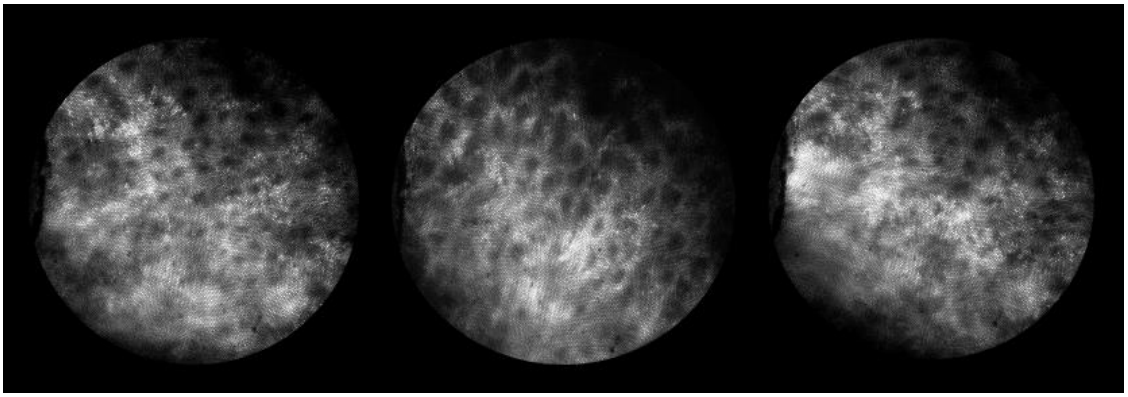

Figure 32. Colon of a healthy mouse seen with the endoscope in-vivo

If we compare results on healthy mice with the results on the AOM/DSS mouse model we can see that the crypts in this last mouse model seems to be larger than the ones on the healthy mouse. The reason could be that, although both are healthy parts of the colon, the area on the AOM/DSS mouse model could have begun to be affected by cancer and the crypts started to destroy increasing in diameter.

4.3. In-vitro and Selective Plane Illumination Microscope results

During in-vivo tests we only see what happens inside the mouse large intestine with the fluorescence fiber-optic endoscope since the mouse was sedated and we did not open it.

The fiber-optic endoscope was tested on healthy fixed mouse colons extracted from mice and in which Acriflavine was previously inserted in the extracted mouse colon. We obtained similar results to those obtained in-vivo. The crypt structure was well appreciated in the whole mouse colon.

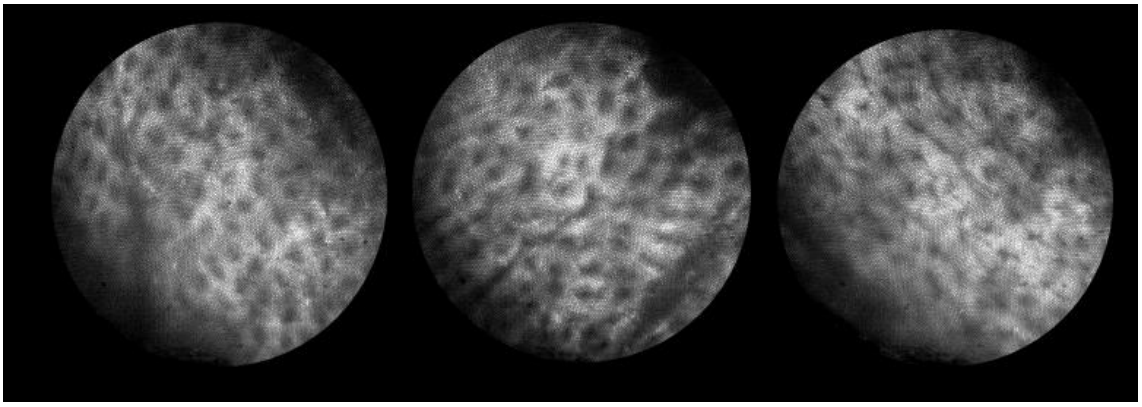

Figure 33. Colon of a healthy mouse seen with the endoscope in-vitro in which we can appreciate the crypt structure of the colon tissue.

Sometimes the crypts we observed under in-vitro tests seems to be smaller than the ones observed under in-vivo tests. This could be due to the fact that since the tissue (mouse colon) was fixed in paraformaldehyde, a polymer, it makes the tissue shrinks

[33] and in many cases this was amplified in some intestines that have been long periods of time in paraformaldehyde (Figure 34).

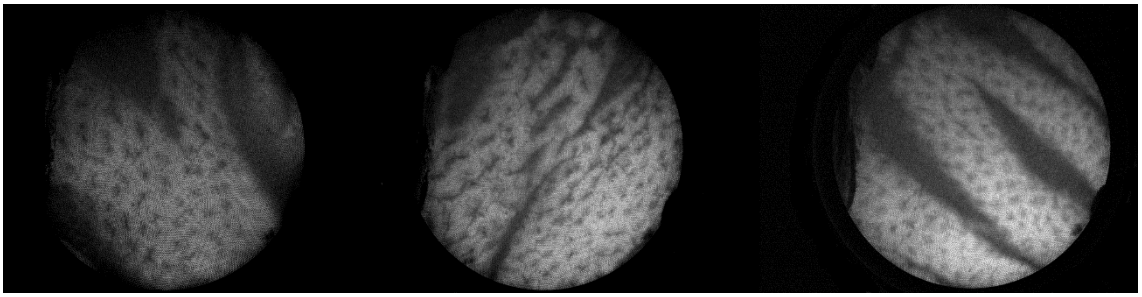

Figure 34. Colon of a mouse seen with the fiber-optic endoscope in-vitro in which we can appreciate the crypt structure of the colon tissue.

In order to prove the results obtained during the in-vivo experiment we sacrificed the mouse and extracted its colon in order to image it under SPIM. As we expected, there were zones in which the colon was tumor-free and zones with tumors in it (Figure 35).

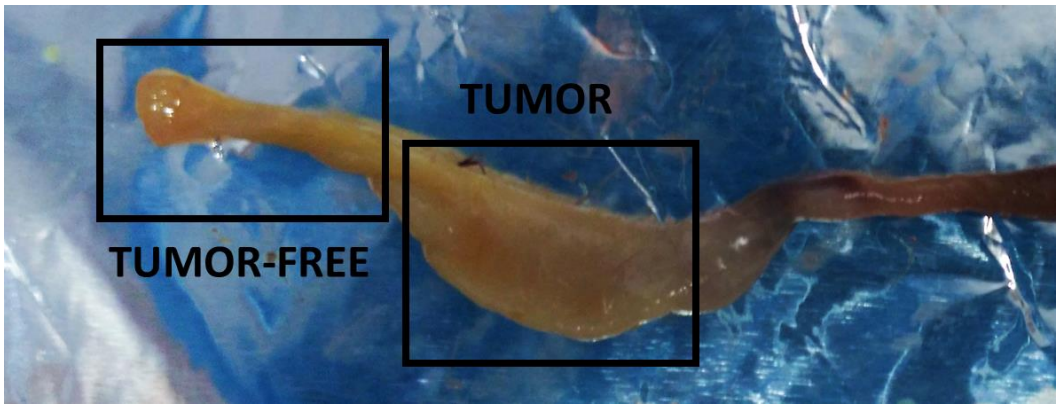

Figure 35. Colon of a mouse in which cancer was induced analyzed with the fiber-optic endoscope in-vivo (before extraction with the mouse alive), in-vitro (after extraction) and under SPIM.

The extracted colon was fragmented in the two different parts identified in Figure 35: a tumor-free fragment and a tumor-bearing fragment that we observed with the fiber-optic endoscope in-vivo. This two fragments were cleared with the CUBIC clearing protocol and examined under SPIM.

Some images of the SPIM under 2x and 5x magnification (Table 2) were analyzed as well as 3D reconstructions of both fragments were performed in ImageJ so that we could appreciate the whole volume structure of both fragments.

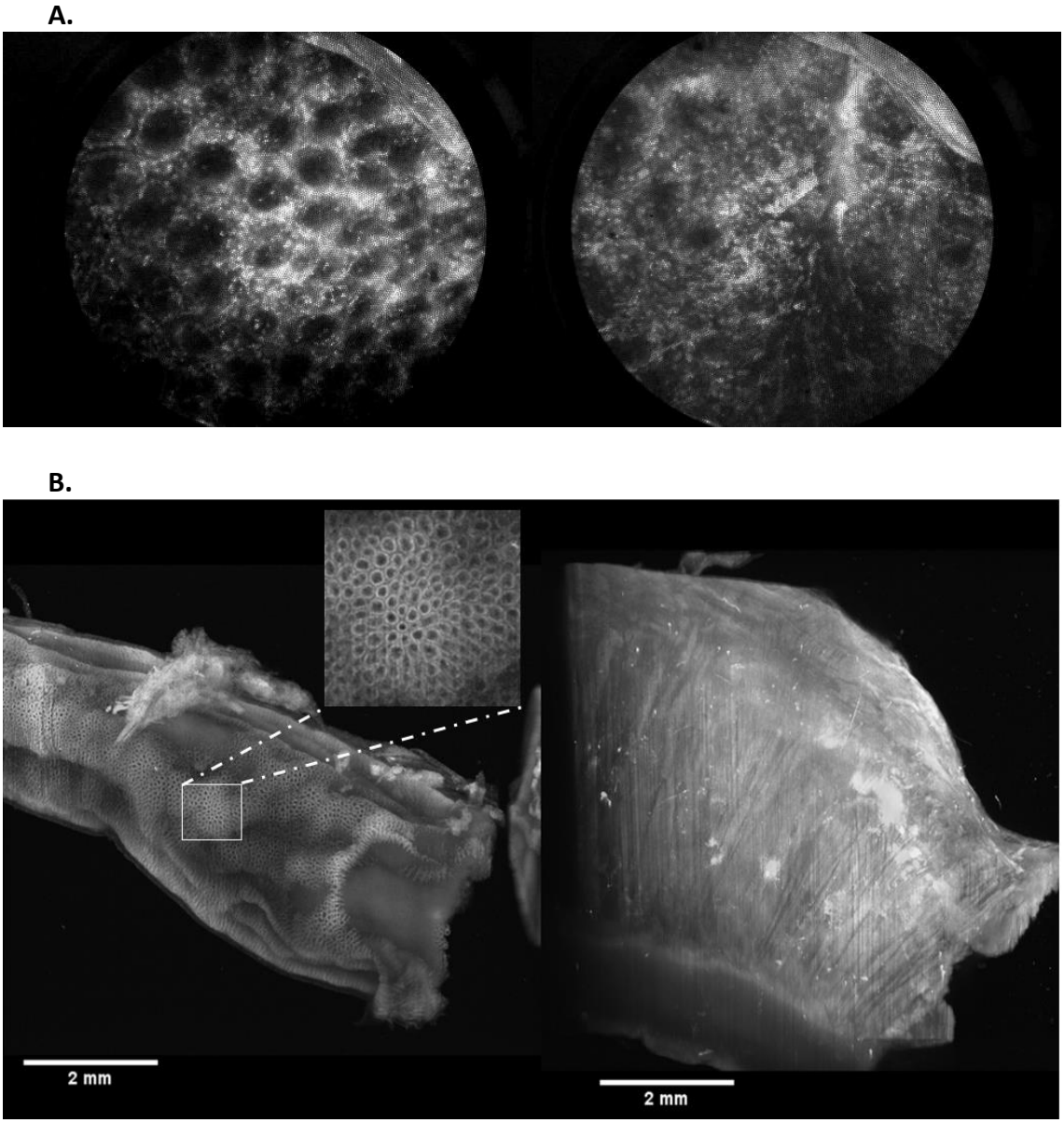

Figure 36. Colon of a mouse. A) Tumor-free fragment (right) and tumor fragment (left) imaged with the fluorescence fiber-optic endoscope in vivo B) Tumor-free fragment (left) and tumor fragment (right) seen under SPIM with a 2x detection objective and 3D reconstructed with ImageJ.

The fragments in Figure 36 correspond to the fragments indicated in Figure 35 and in which we could easily appreciate the difference in size between the tumor fragment (larger) and the tumor-free fragment.

The SPIM results showed us the same results as the ones obtained during the in-vivo experiment. SPIM images showed us that the tumor-free part of the intestine had the crypt structure preserved and the tumor fragment did not show any crypt structure and only tendons were appreciated (Figure 36 and Figure 37).

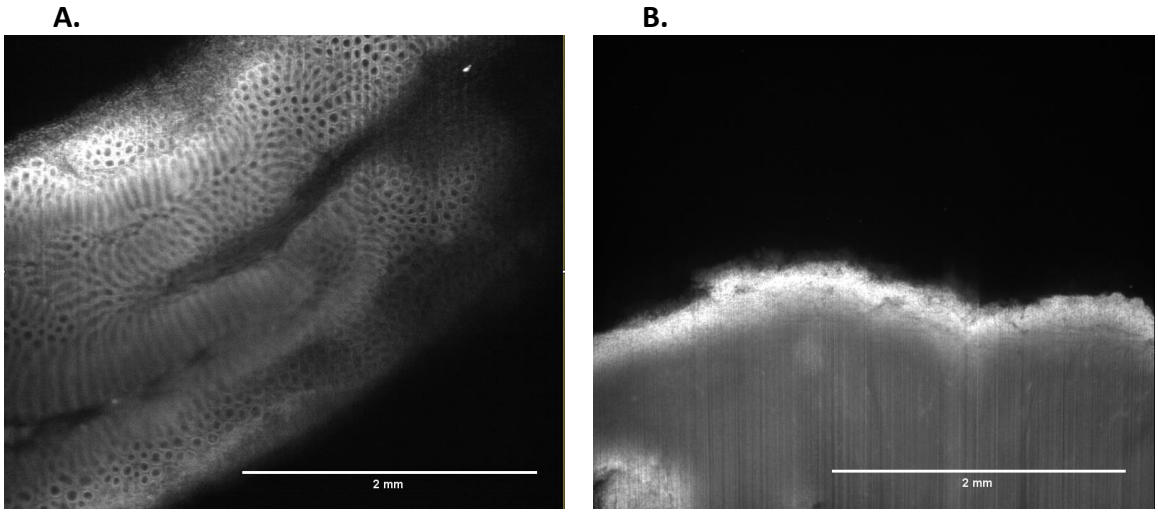

Figure 37. Fragments of the colon of a mouse seen under SPIM with a 5x detection objective. A) Tumor-free fragment in which we can appreciate the crypt structure and B) Tumor fragment in which we cannot see any tissue structure.

More in-vivo and in-vitro tests were performed in healthy mice in order to test the quality and resolution of the fiber-optic endoscope. Furthermore, these tests allowed us to prove that the crypt structure of the colon tissue can be appreciated with the fluorescence fiber-optic endoscopy system, so that the results obtained with the AOM/DSS mouse model and healthy mice in-vivo, in-vitro and under SPIM gave us real results of the structure of the colon tissue.

5. CONCLUSIONS

A high resolution fiber-optic endoscope has been developed and improved during this project for the colorectal tissue research in mice. The real application in mice has been demonstrated with some in-vivo tests in healthy mice as well as in a cancer induced mouse model.

Two different fiber bundles have been used: one with the nude tip and the other with a GRIN lens attached to the tip. Some experiments in-vivo and in-vitro were performed in order to see the application of the two different fibers and we reach to the conclusion that the GRIN lens fiber was not appropriate for an endoscopy due it cannot focus on the 3D structure of the colon tissue. We only obtained good results with the fiber bundle without the GRIN lens that are the ones shown in the results.

One in-vivo test was done on an AOM/DSS mouse model that is usually used for the colon carcinogenesis and chemo preventive intervention studies in humans. This model chemically induces colorectal cancer in mice causing the destruction of the colon tissue. The in-vivo test has shown that, as expected, there were areas of the colon where the characteristic crypt structure of the intestine tissue has been preserved while other parts of the colon that have been affected by cancer and in which the tissue structure has been destroyed.

The in-vivo results were validated with in-vitro tests with the florescence fiber-optic endoscope and with a SPIM test on the AOM/DSS mouse model colon of the mouse tested in-vivo.

The illumination source of the fiber-optic endoscope has been improved by comparing a laser and a LED as light sources for the system. We reached to the conclusion that the LED source was better in gain and exposure times so we finally keep it as the definitive light source for the fluorescence fiber-optic endoscope.

The resolution of the fiber-optic endoscope system has been calculated and a calibration protocol for the system has been defined.

With this project we have proved that the fluorescence fiber-optic endoscope developed is appropriate for in-vivo studies of colorectal cancer in mice, being optimal in the detection of the cellular structure (crypts) of the large intestine (colon).

6. FUTURE WORK

Future improvements of the system will consist mainly on increasing the number of excitation and emission wavelengths that the system may detect, if possible simultaneously. This will be done either by selecting which wavelength to use via a motorized system with different filters, or by modulating the excitation light in order to separate the contributions later via software, using what is termed “multiplexing”. This would enable imaging several fluorophores simultaneously, offering additional molecular and anatomical information. The system in its current form does not provide anatomical information and may only provide florescent measurements. By introducing the “multiplexing” approach, full RGB images superimposed to the fluorescence images may be formed making use of a single fiber bundle.

With respect to the practical use of the system, a soft tip will be attached to the fiber bundle in order to reduce the damage that the tip makes in the tissue when in direct contact.

PROJECT COSTS

The budget of this project was estimated taking into account four different types of resources: Endoscope components, technical equipment, laboratory material and human resources.

Endoscope components	Quantity	Cost/Units	Total Cost
Fiber bundle: FIGH-30-850N, Fujikura, Koto, TKY, Japan	1	621,83 €	621,83 €
Fiber bundle with GRIN lens: FIGH-30-850N, Fujikura, Koto, TKY, Japan	1		
Allied Vision Manta G-145-30fps 2/3" Color CCD Camera: Edmund optics, Newport, NJ, USA	1	2.133,03 €	2.133,03 €
LB1945-A-ML - Mounted N-BK7 Bi-Convex Lens, Ø1", f = 200.0 mm, ARC: 350-700 nm: Thorlabs Inc, Delaware, USA	1	38,84 €	38,84 €
ACL2520U - Aspheric Condenser Lens, Ø25 mm, f=20.1 mm, NA=0.60	1	20 €	20 €
Dichroic Mirror and Emission : Edmund optics, Newport, NJ, USA	1	556,64 €	556,64 €
Bandpass Filter, CWL = 400 ± 8 nm, FWHM = 40 ± 8 nm: Thorlabs Inc, Delaware, USA	1	99,00 €	99,00 €
RMS10X - 10X Olympus Plan Achromat Objective, 0.25 NA, 10.6 mm WD Thorlabs Inc, Delaware, USA	1	349,20 €	349,20 €
M405D2 - UV (405 nm) LED on Metal-Core PCB, 1400 mA, 1500 mW (Min): Thorlabs Inc, Delaware, USA	1	165,00 €	165,00 €
Box of the system	1	200 €	200 €
			Total: 4183,54 €

Table 4. Endoscope components asscociated costs

The costs generated by the technical equipment include laboratory machinery, the SPIM microscope as well as the different software and the computer hardware used in this project such as ImageJ or LabVIEW.

Technical equipment	Quantity	Costs/Units	Depreciation/Month	Months employed	Total Cost
SPIM	1	120 000 €	1.000 €	2	2.000 €
Personal Computer	1	700 €	10 €	9	90 €
University Computer	1		10 €	6	60 €
Engine	1	0	0	5	0
LabVIEW Software	1	0	0	9	0
ImageJ Software Office Word 2013	1	0	0	9	0
Zaber Console Software	1	0	0	1	0
					Total: 2.150 €

Table 5. Technical equipment associated costs

The budget for laboratory material includes all clearing reagents including PBS, Triton, urea, sucrose, detergents and polyalcohols; fluorescent labeling such as Alexa Fluor 647, DAPI or Acriflavine as well as expendable material. Consumable laboratory material includes everyday items used for the sample clearing protocols such as 50 mL Falcon tubes, Pasteur pipettes, multiwall culture plates, etc. This material is supplied directly at the Centro de Biologia Molecular Severo Ochoa.

Laboratory Material	Quantity	Costs/Unit	Total Cost
Clearing Reagents: Sigma Aldrich	1	400 €	400 €
Acriflavine: Sigma Aldrich	1 (10g)	40,50 €	40,50 €
Alexa Fluor 647 Phalloidin: ThermoFischer	2	43 €	86 €
DAPI: Sigma Aldrich	2	3,5 €	7 €
Consumable laboratory material	---	70 €	70 €
Mouse	4	20 €*	80 €
Dextran sodium sulphate (DSS) agent: MP Biomedicals	1 (10g)	126 €	126 €

Azoxymethane (AOM) A5486-25MG: Sigma	1	270,50 €	270,50 €
			Total: 1.080 €

**** 6 weeks of life mouse***

Table 6. Laboratory material associated costs

Human resources costs comprise the salaries of the team members working on the project. In this case, the student and the tutor worked full time while the Co-tutor worked part-time and one more person offered consulting hours occasionally. I consider an average salary for the student of 25€/hour, an average salary for the tutor and co-tutor as engineer and biologist of 40€/hour and an average salary for the assistant post-bachelor of 30€/hour.

Human Resources	Months	Cost/Month	Total
Student	8	750 €	6.000 €
Tutor	8	1200 €	9.600 €
Co-tutor	5	1200 €	6.000 €
Assistant	2	900 €	1800 €
			Total: 23.400 €

Table 7. Human resources associated costs.

Concept	Total Cost
Endoscope componets	4183,54 €
Technical equipment	2.150 €
Laboratory material	1.080 €
Human Resources	23.400€
	Total Project Cost: 30813, 54 €

Table 8. Total Project cost

ANNEX

LabVIEW Program

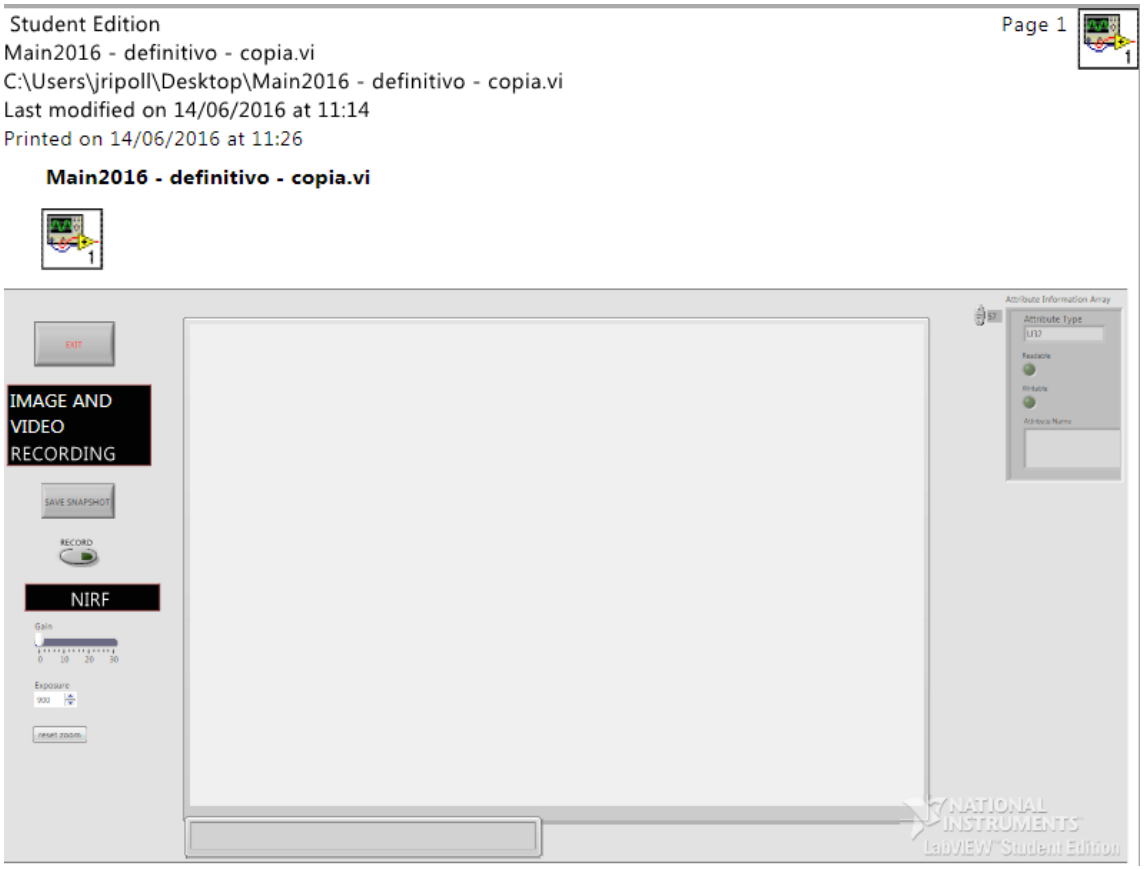

Figure 38. Control Window of the LabVIEW program

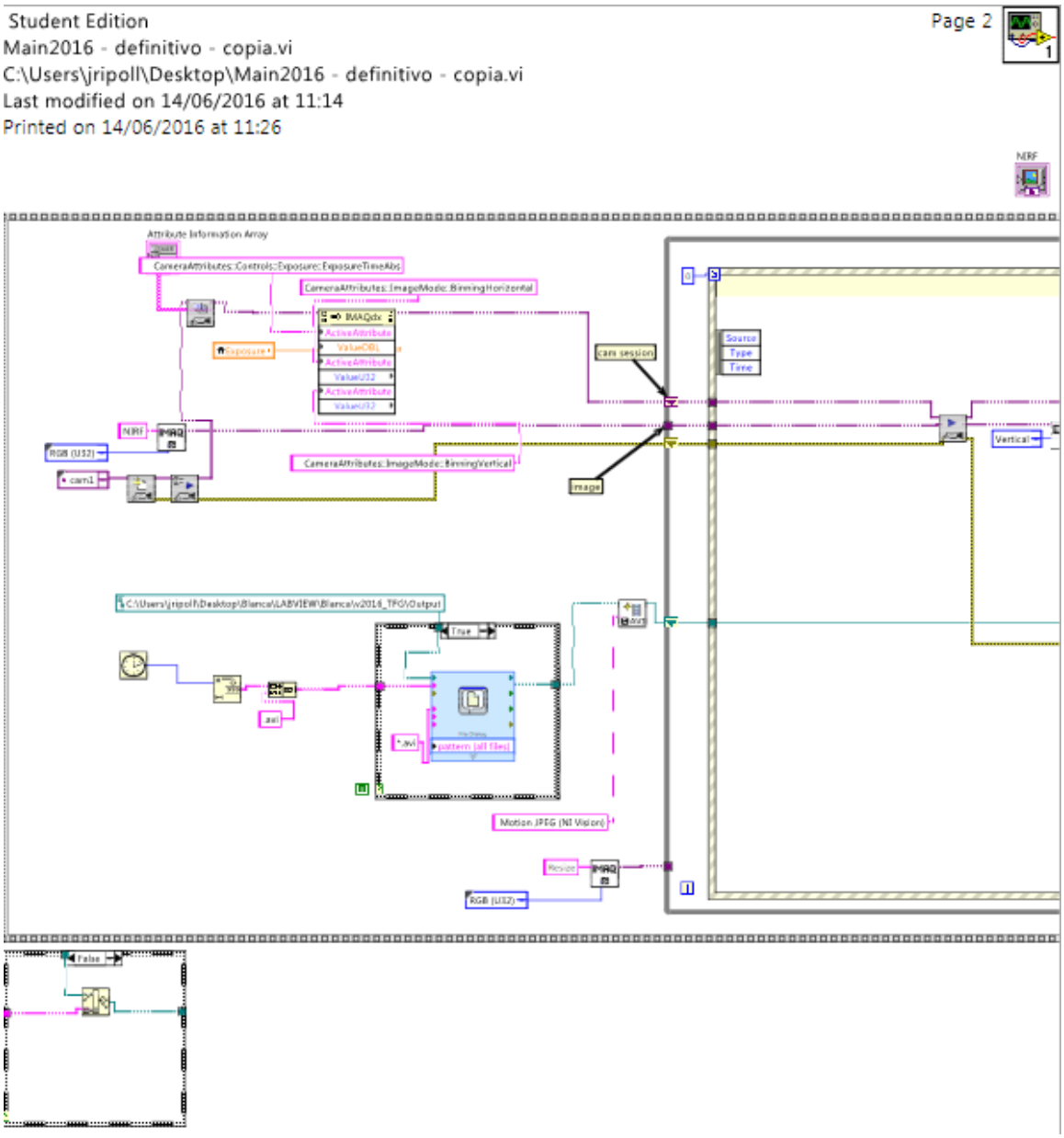

Figure 39. Terminal Window of the LabVIEW program

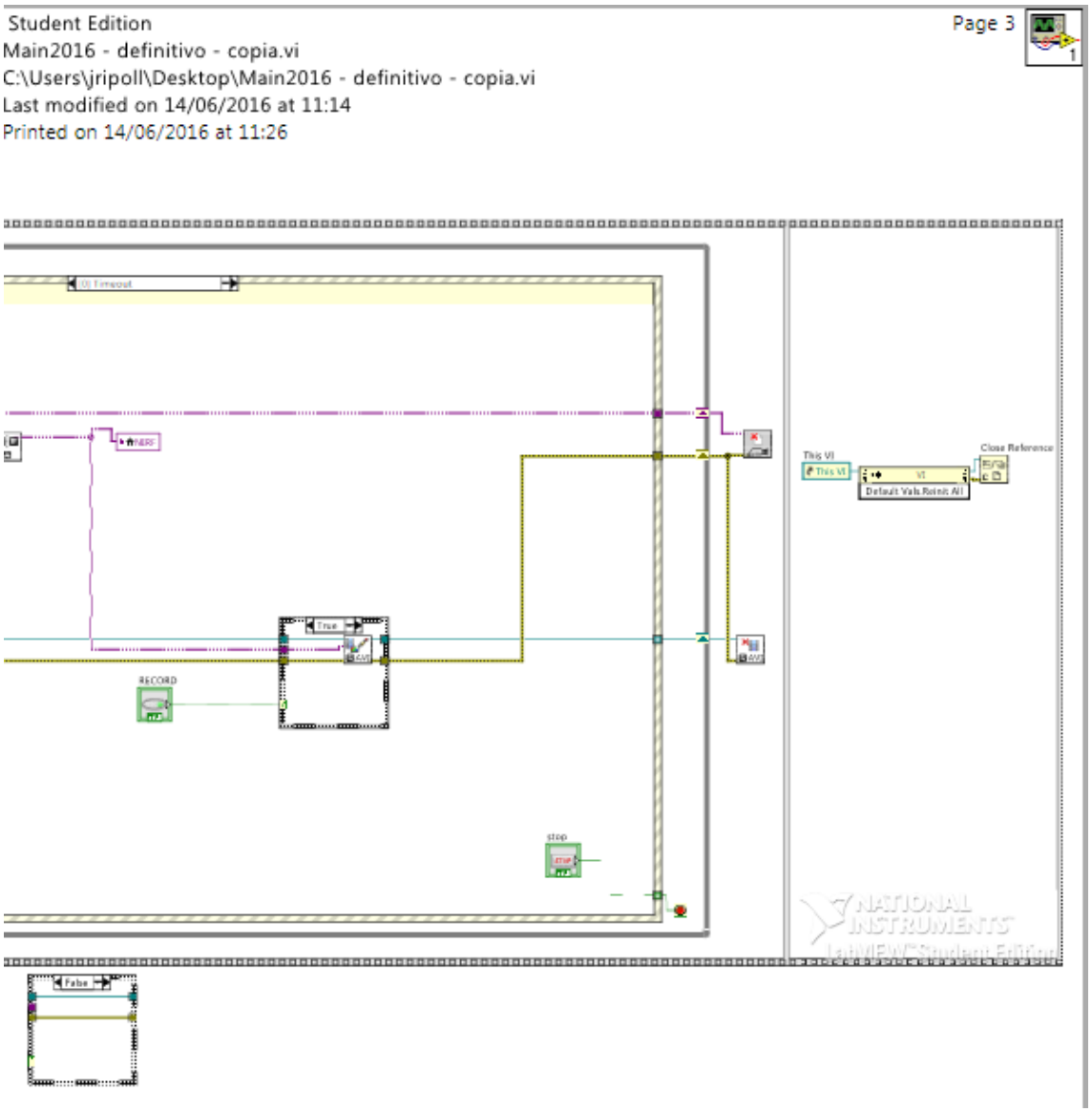

Figure 40. Terminal Window of the LabVIEW program

Reference Sheet

Fiber-optic Endoscope Protocol for its use and calibration.

1. Connect the fiber-optic endoscope cage (from behind) to the power supply with a power cord.
2. Connect the fiber-optic endoscope cage (from behind) to the computer with an ethernet cable.
3. Assemble the desired fiber-optic (with our without GRIN lens) to the fiber-optic coupling of the endoscope cage.
4. Turn on the power supply of the endoscope cage with the power button located in the back of the endoscope cage.
5. Turn on the LED power supply with the power button located in the front part of the endoscope cage. Once this step is done, the laser light should be seen at the tip of the optical fiber already connected.

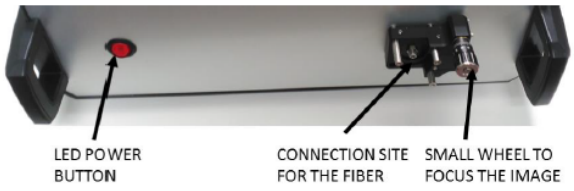

6. Open the LabVIEW program in the computer and run the program to start acquiring real time videos.
7. Point the fiber bundle at the lights so that you are able to see a homogeneous image.

Universidad Carlos III de Madrid · SaludMadrid · Hospital General Universitario Gregorio Marañón · Comunidad de Madrid · CBM Severo Ochoa

8. Focus the image with the small wheel located in the fiber-optic coupling in the front part of the cage as we can see in (Figure 19). This small wheel moves the fiber-optic coupling in very little distances so that we can perfectly obtain a focused image in which we can easily see the individual cores.

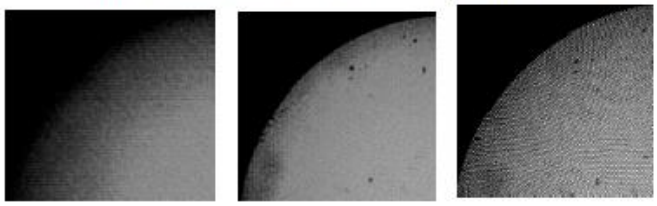

9. Improve quality of the image with the bar GAIN  and the changing values box  EXPOSURE of the LabVIEW program and save images or record videos with SAVE  and RECORD  buttons respectively.
10. Once we want to stop viewing the real time images we should stop the capture of images with EXIT 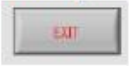 button that stops the program.

11. Clean the fiber bundle with isopropanol to remove dust before and after each use.

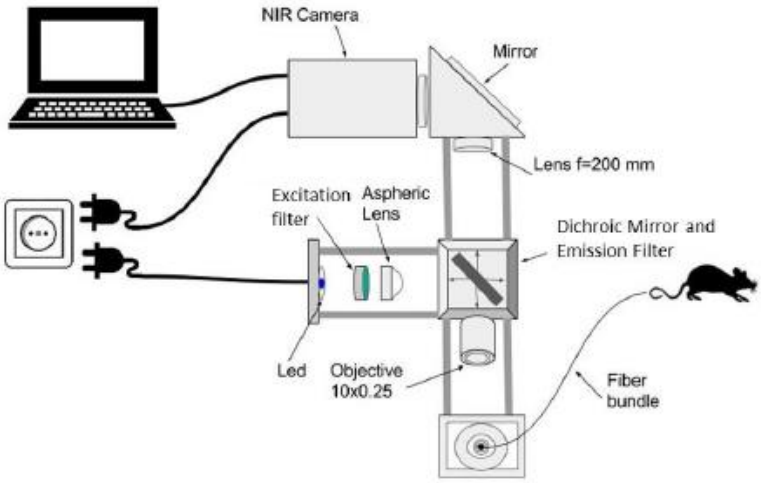

Publications

Part of the in-vitro validation with Light Sheet Microscopy of the colon tissue performed at the CBM were submitted for publication to the SPIE Photonics West 2016 Conference, San Francisco (California, USA): 'The Cubic Protocol adapted for 3D imaging of the intact murine colon with light sheet microscopy'

The Cubic Protocol adapted for 3D imaging of the intact murine colon with light sheet microscopy

B. Zufiria[a,b], D.I. Bocancea[b,c], M. V. Gómez-Gaviro[b,c], M. Desco[b,c], M. Fresno[a], J. Ripoll *[b,c], and A. Arranz* [a]

[a] Center for Molecular Biology "Severo Ochoa" (CBMSO), CSIC-Universidad Autónoma de Madrid, Madrid, Spain.

[b] Department of Bioengineering and Aerospace Engineering, Universidad Carlos III of Madrid, Madrid 28911, Spain

[c] Experimental Medicine and Surgery Unit, Instituto de Investigación Sanitaria Gregorio Marañón, 28007 Madrid, Spain

ABSTRACT

We here show 3D light sheet microscopy images of fixed and cleared murine colon tissue *in-toto*, which offer cellular information without the need for physically sectioning the tissue. We have adapted and applied the recently developed CUBIC protocol (Susaki et al. Cell 157:726, 2014) for colon tissues and have found that this clearing protocol enables imaging all the way to the central part of the lumen with cellular resolution, thus opening new ways for 3D imaging of colon samples with application in studies of gut inflammation and colon carcinoma.

Keywords: light sheet Microscopy, CUBIC protocol, tissue clearing, immune response, inflammation

1. INTRODUCTION

Light sheet microscopy or Ultramicroscopy, originally developed in 1903[5], was first applied in 1983 to fixed and cleared tissue as Orthogonal-plane Fluorescence Optical Sectioning (OPFOS) [6], as Thin Laser Sheet imaging microscopy (TSLIM) in 2002[7], and finally applied to whole fixed and cleared tissues as Ultramicroscopy [8]. Its use *in vivo* was first presented by Huisken *et al* in 2004[9] as Selective Plane Illumination Microscopy (SPIM), applied to *in-vivo* zebrafish imaging. Light Sheet Microscopy is based on generating a thin sheet of light within the specimen and making this sheet of light coincide with the focal plane of an objective (see [10] and the special issue of Nature Collections[11] for a review on Light Sheet Microscopy). Its contrast is based on fluorescence, and in order to implement light sheet microscopy we need to access the sample at 90deg with the excitation source. There are several ways of generating this light sheet, the original setups making use of cylindrical lenses, while further developments made use of structured illumination such as Digitally Scanned Light Sheet Microscopy (DSLM)[12] and DSLM-SI[13], sometimes combined with multi-photon excitation in order to improve resolution even further[14–16].

However, when imaging whole tissue samples with light sheet microscopy, the scattering of the sample is a major limiting factor to obtain 3D-images. In order to overcome this limitation, different clearing methods such as CUBIC (clear, unobstructed brain imaging cocktails) have been developed to increase the transparency of the samples, enabling the 3D-imaging of whole organs with cellular resolution. CUBIC allows the clearing of samples without disturbing endogenous fluorescent signal. Since its publication in 2004 by Susaki et al[1,2], the CUBIC protocol has been extensively used for clearing a wide range of tissues (see, for example, Ref. [3]), allowing 3D imaging of in-toto samples. This has provided new tools for studying a variety of tissue samples with high resolution and without sectioning. In this work, we will focus in adapting the CUBIC protocol for mouse colon tissue, as the targeted sample in studies of intestinal inflammation and colon carcinoma. Once cleared, the ideal imaging technique to image such large tissue sample is Light Sheet Microscopy.

* alicia.arranz@cbm.csic.es, phone: +34 911964572; jorge.ripoll@uc3m.es, phone: +34 916248198.

2. MATERIALS AND METHODS

2.1 Light Sheet Microscopy

The setup used for light sheet microscopy has been developed in-house at the Universidad Carlos III de Madrid, and is depicted in Figure 1. It consists on a laser unit comprising 405nm, 480nm, 530nm, 598nm and 635nm laser lines (CNI lasers, China), with powers ranging from 50mW to 200mW. Using rotation motor controlled from the PC using custom software (see below), we are able to select which laser line is to be used, being possible only to image one laser line at a time. The selected laser exits the laser unit and its intensity is controlled via a filterwheel with several optical density filters, enabling reduction of its intensity between 3 orders of magnitude and 50%. This beam is then steered towards a cylindrical lens (f=50mm, Thorlabs, USA) which is focused onto the back-aperture of a 5x Long working distance objective (Mitutoyo, Japan). This creates a light sheet of approximately 2um in the cuvette used for immersion. This cuvette, filled with CUBIC reagent II, is then imaged using either a 2x, 5x or a 10x long working distance objective (Mitutoyo, Japan). An emission filter wheel is placed immediately behind the detection objective (note that the focal plane of this detection objective needs to coincide with the light sheet generated by the cylindrical lens / illumination objective combination), containing 25mm diameter filters, one specific for each laser line. The image is then formed onto the chip of a CMOS camera (NEO, Andor, Northern Ireland) by means of a tube lens place after the emission filter wheel.

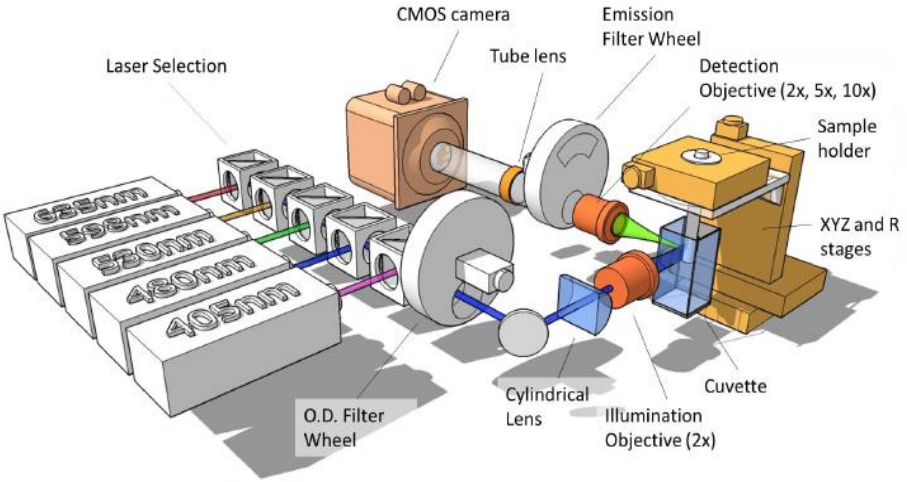

Figure 1. Multispectral Light Sheet Microscope

2.2 Sample preparation

All procedures described here were approved by the CBM-UAM's Ethics Committee (Madrid, Spain) and complied with National and European Union legislation. Mice were housed at the animal facility in the CBM. Prior collection of tissue samples, animals were deeply anesthetized and euthanized. Colon tissue was aseptically removed, washed and flushed with PBS and fixed in 4% PFA for at least 24h at 4ºC. After fixation, samples were washed twice with PBS (2x 10 min) and the CUBIC protocol was followed.

2.3 CUBIC Protocol

In order to clear colon tissue samples the CUBIC protocol was followed [2], optimized for colon tissue samples. After testing different incubation times, 48h in CUBIC reagent I (25 wt% urea, 25 wt% N,N,N',N'-tetrakis(2-hydroxypropyl)ethylenediamine, and 15 wt% Triton X-100, all from Sigma Aldrich, Spain) and 48h in CUBIC reagent II (50 wt% sucrose, 25 wt% urea, 10 wt% 2,20,20'-nitrilotriethanol, and 0.1% (v/v) Triton X-100, all from Sigma Aldrich, Spain) resulted sufficient for successfully clearing the mouse colon sample (Figure 2).

Briefly, samples were kept in CUBIC reagent I for 48h at 37ºC with gentle shaking, washed with PBS (3x 10min) and stained with DAPI (Merk Millipore, 1:5000), and Actin-green (ThermoFischer, 1:100) for 24h. Samples were then washed again with PBS (3x 10min), incubated in 30% sucrose at room temperature for 30 min (or until the sample was completely submerged) and then kept in CUBIC reagent II for at least 48h at 37ºC with gentle shaking, prior to imaging.

Figure 2. Example of cleared colon tissue following the cubic protocol.

3. RESULTS AND DISCUSSION

We have successfully managed to clear mouse colon tissue samples using an adapted CUBIC protocol. Given the specific characteristic of the intestinal tissue (its "tubular" shape, which allows a better contact with the CUBIC reagents), we were able to reduce the time for the clearing procedure to 5 days. However, this "tubular" shape was also the reason of an additional difficulty as bubbles were appearing in the lumen of the samples during the different incubations in the washing and clearing reagents. In order to avoid that, flushing the lumen with the different buffers and clearing reagents was required prior to the incubation of the samples.

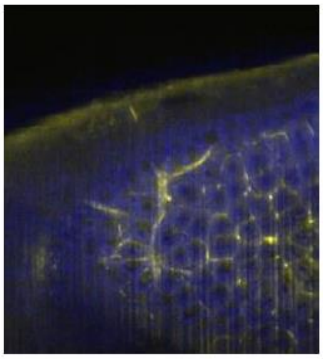

Following this procedure, we were able to increase the transparency of mouse colon tissue samples, allowing the imaging of a large portion of colon tissue sample using Light Sheet Microscopy. As an example and as a control experiment, we imaged mouse colon tissue stained with DAPI, which labels cell nuclei, and Actin-green, which labels filamentous actin (Figure 3 and 4). Since one of the main goals of our applications is to be able to analyze large colon tissue samples, low magnifications and large fields of view are an advantage. However, it must be noted that higher resolution images may be obtained with this approach, by generating thinner light sheets and using higher magnification detection.

Figure 3. Detail of colon tissue imaged with a 5x objective, stained with Actin-green (in yellow, labelling filamentous actin) and DAPI (in blue, labelling cell nuclei).

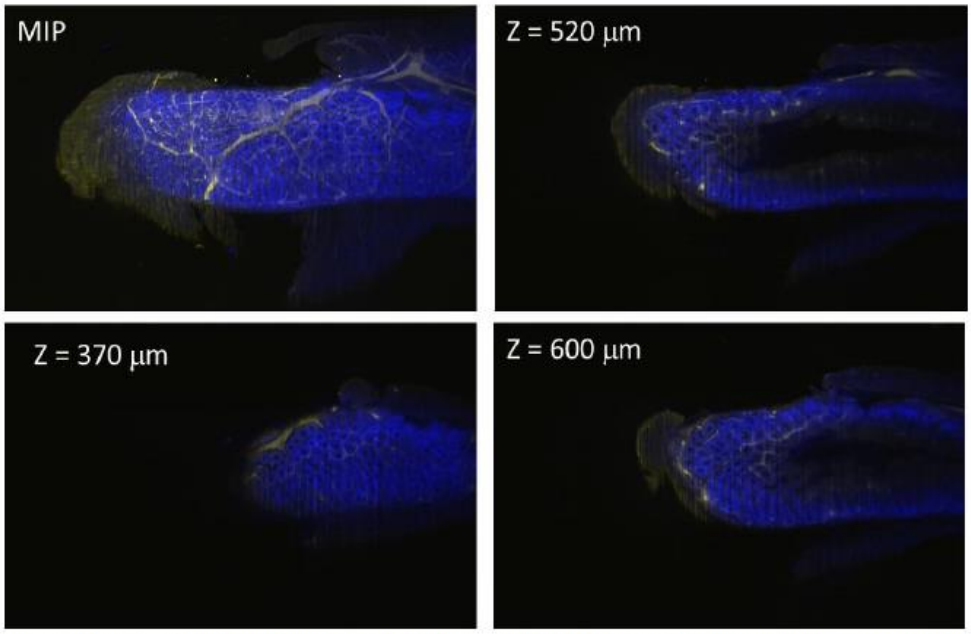

Figure 4. 3D Light sheet microscopy images of colon tissue labelled for filamentous actin (with Actin-green, in yellow) and cell nuclei (with DAPI, in blue).

4. CONCLUSIONS

We have demonstrated that Light Sheet Microscopy combined with an adapted CUBIC protocol offers new ways of studying mouse colon tissue with cellular resolution. As a significant advantage, it must be stated that the CUBIC protocol retains any endogenous fluorescence that might be present, thus allowing the use of transgenic animals expressing fluorescence proteins. Future work will consist on using CUBIC and light sheet microscopy on transgenic animals expressing fluorescence proteins under the control of specific gene promoters involved in inflammation and cancer development.

ACKNOWLEDGEMENTS

This project was funded by EC FP7 CIG grant HIGH-THROUGHPUT TOMO and the Spanish MINECO project grant FIS2013-41802-R MESO-IMAGING. J.R. wishes to acknowledge support from EC H2020 Marie Curie IEF grant SURREALISM.

REFERENCES

[1] Susaki, E.A., Tainaka, K., Perrin, D., Yukinaga, H., Kuno, A., and Ueda, H.R., "Advanced CUBIC protocols for whole-brain and whole-body clearing and imaging," Nature Protocols 10(11), 1709–1727 (2015).

[2] Susaki, E. a, Tainaka, K., Perrin, D., Kishino, F., Tawara, T., Watanabe, T.M., Yokoyama, C., Onoe, H., Eguchi, M., et al., "Whole-brain imaging with single-cell resolution using chemical cocktails and computational analysis.," Cell 157(3), 726–39 (2014).

[3] Masson, A., Escande, P., Frongia, C., Clouvel, G., Ducommun, B., and Lorenzo, C., "High-

resolution in-depth imaging of optically cleared thick samples using an adaptive SPIM.," Scientific reports 5, 16898 (2015).

[4] Kelch, I.D., Bogle, G., Sands, G.B., Phillips, A.R.J., LeGrice, I.J., and Rod Dunbar, P., "Organ-wide 3D-imaging and topological analysis of the continuous microvascular network in a murine lymph node.," Scientific reports 5, 16534 (2015).

[5] Siedentopf, H., and Zsigmondy, R., [Über Sichtbarmachung und Größenbestimmung ultramikroskopischer Teilchen, mit besonderer Anwendung auf Goldrubingläser] , in Ann. der Phys. 10, 1–39 (1903).

[6] Voie, a H., Burns, D.H., and Spelman, F. a, "Orthogonal-plane fluorescence optical sectioning: three-dimensional imaging of macroscopic biological specimens.," Journal of microscopy 170(Pt 3), 229–36 (1993).

[7] Fuchs, E., Jaffe, J., Long, R., and Azam, F., "Thin laser light sheet microscope for microbial oceanography," Optics Express 10(2), 145 (2002).

[8] Dodt, H., Leischner, U., and Schierloh, A., "Ultramicroscopy: three-dimensional visualization of neuronal networks in the whole mouse brain," Nature methods 4(4), 331–336 (2007).

[9] Huisken, J., Swoger, J., and Bene, F. Del, "Optical sectioning deep inside live embryos by selective plane illumination microscopy," Science 1007(2004), (2004).

[10] Weber, M., Mickoleit, M., and Huisken, J., "Light sheet microscopy," Methods in cell biology 123, 193–215 (2013).

[11] "Light-Sheet Microscopy , December 2013," Nature Collections 1, .

[12] Keller, P., Schmidt, A., Wittbrodt, J., and Stelzer, E., "Reconstruction of zebrafish early embryonic development by scanned light sheet microscopy," Science 322(November), 1065–1069 (2008).

[13] Keller, P.J., Schmidt, A.D., Santella, A., Khairy, K., Bao, Z., Wittbrodt, J., and Stelzer, E.H.K., "Fast, high-contrast imaging of animal development with scanned light sheet-based structured-illumination microscopy.," Nature methods 7(8), 637–42 (2010).

[14] Gao, L., Shao, L., Chen, B.-C., and Betzig, E., "3D live fluorescence imaging of cellular dynamics using Bessel beam plane illumination microscopy.," Nature protocols 9(5), 1083–101 (2014).

[15] Gao, L., Shao, L., Higgins, C.D., Poulton, J.S., Peifer, M., Davidson, M.W., Wu, X., Goldstein, B., and Betzig, E., "Noninvasive Imaging beyond the Diffraction Limit of 3D Dynamics in Thickly Fluorescent Specimens," Cell 151(6), 1370–1385 (2012).

[16] Planchon, T.A., Gao, L., Milkie, D.E., Davidson, M.W., Galbraith, J.A., Galbraith, C.G., Betzig, E., and Catherine, G., "Rapid three-dimensional isotropic imaging of living cells using Bessel beam plane illumination," Nature methods 8(5), 417–423 (2011).

BIBLIOGRAPHY

[1] Board, C. N. E. (2015). Cáncer colorrectal - Estadísticas. Retrieved from http://www.cancer.net/es/tipos-de-cáncer/cáncer-colorrectal/estadísticas

[2] American Cancer Society. (2015). When is endoscopy used? Retrieved from http://www.cancer.org/treatment/understandingyourdiagnosis/examsandtestdescriptions/endoscopy/endoscopy-when-is-endoscopy-used

[3] Melina, R. (2010). Why Do Medical Researchers Use Mice? *Livescience*. Retrieved from http://www.livescience.com/32860-why-do-medical-researchers-use-mice.html

[4] DifferenceBetween. (n.d.). Difference Between a Human Digestive System and a Rat Digestive System. Retrieved from http://www.differencebetween.net/science/difference-between-a-human-digestive-system-and-a-rat-digestive-system/

[5] Nguyen, T. L. A., Vieira-Silva, S., Liston, A., & Raes, J. (2015). How informative is the mouse for human gut microbiota research? *Disease Models and Mechanisms*, *8*(1), 1–16. Retrieved from http://dmm.biologists.org/content/8/1/1.figures-only

[6] Fujii, M., & Sato, T. (2014). Culturing intestinal stem cells : applications for colorectal cancer research. http://doi.org/10.3389/fgene.2014.00169

[7] Wikipedia contributors. "Endoscopy." *Wikipedia, The Free Encyclopedia*. Wikipedia, The Free Encyclopedia, 15 Jun. 2016. Web. 15 Jun. 2016. Retrieved from https://en.wikipedia.org/wiki/Endoscopy#Applications

[8] Dimensions, E. (n.d.). Anatomy & Physiology of a Flexible Scope: Anatomical Structure. Retrieved from https://www.educationaldimensions.com/eLearn/endoscope/anatomy.php

[9] Woodford, C. ExplainThatStuff. (n.d.). Endoscopes. 16 April, 2016. Retrieved from http://www.explainthatstuff.com/endoscopes.html

[10] Spach, D. H., Silverstein, F. E., & Stamm, W. E. (1993). Transmission of Infection by Gastrointestinal Endoscopy and Bronchoscopy. *Annals of Internal Medicine*, *118*(2), 117–128. Retrieved from http://dx.doi.org/10.7326/0003-4819-118-2-199301150-00008

[11] Skin, Ja. 6. . & C. (n.d.). Fiber-optic endoscopy. Retrieved from http://130.237.83.53/medicaldevices/album/Ch 7 Medical images/slides/F 7-4 Fiber optic endoscopy.html

[12] Robot Builder's Bonanza. (n.d). Touch Sensitivity with Laser Fiber 'Whiskers'. Retrieved from http://www.robotoid.com/appnotes/sensors-laser-fiber-whiskers.html

[13] Huisken, J., & Stainier, D. Y. R. (2009). Selective plane illumination microscopy techniques in developmental biology. *Development*, *136*(12), 1963–1975. Retrieved from http://dev.biologists.org/content/136/12/1963.abstract

[14] Borlinghaus. R, Multer. A, *Leica Mircosystems* (2014). Clearing procedures for deep tissue imaging. Retrieved from http://www.leica-microsystems.com/science-lab/clarity/clearing-procedures-for-deep-tissue-imaging/

[15] Ueda, H. (2014). Rapid whole-brain imaging with single cell resolution. Retrieved from http://www.riken.jp/en/pr/press/2014/20140418_1/#

[16] Chen, Z., Zhu, N., Pacheco, S., Wang, X., & Liang, R. (2014). Single camera imaging system for color and near-infrared fluorescence image guided surgery. *Biomedical Optics Express*, *5*(8), 2791–2797. http://doi.org/10.1364/BOE.5.002791

[17] Edmund Optics. (n.d.). All About Aspheric Lenses. Retrieved from http://www.edmundoptics.com/resources/application-notes/optics/all-about-aspheric-lenses/

[18] Wikipedia contributors. Aspheric lens [Internet]. Wikipedia, The Free Encyclopedia; 2016 May 6, 09:02 UTC [cited 2016 Jun 15]. Available from: https://en.wikipedia.org/w/index.php?title=Aspheric_lens&oldid=718899129.

[19] Thorlabs. (n.d.-c). *RMS10X - 10X Olympus Plan Achromat Objective, 0.25 NA, 10.6 mm WD*. Retrieved from http://www.thorlabs.de/thorproduct.cfm?partnumber=RMS10X

[20] Ockenga, W. (2011). Fluorescence in Microscopy. Retrieved from http://www.leica-microsystems.com/science-lab/fluorescence-in-microscopy/

[21] Optics, E. (n.d.). 458nm, 25.2 x 35.6mm, Dichroic Filter. Retrieved from http://www.edmundoptics.es/optics/optical-filters/longpass-edge-filters/fluorescence-dichroic-filters/67078/

[22] Fujikura. (n.d.-b). Image Fibre. Retrieved from http://www.fujikura.co.uk/products/medical-industrial-optical-fibre/image-fibre/

[23] Fujikura. (n.d.-a). Image Fiber. Retrieved from http://www.fujikura.co.jp/eng/products/optical/appliedoptics/03/2050110_12902.html

[24] TECH, G. (n.d.). Gradient Index Optics. Retrieved from http://www.grintech.de/gradient-index-optics.html

[25] Thorlabs. (n.d.-a). LED on Metal-Core PCB, 1400 mA, 1500 mW (Min). Retrieved from http://www.thorlabs.de/thorproduct.cfm?partnumber=M405D2

[26] National Instruments. (n.d.). LabVIEW. Retrieved from http://www.ni.com/labview/esa/

[27] Manual, U. (2004). TM IMAQ Vision for LabVIEW. *North*, *88*(371007), 331–339. http://doi.org/10.1017/S0025315408000659

[28] Thorlabs. (n.d.-b). Resolution Test Targets. Retrieved from http://www.thorlabs.de/newgrouppage9.cfm?objectgroup_id=4338

[29] Robertis, M. De, Massi, E., Poeta, M. L., Carotti, S., Morini, S., Cecchetelli, L., … Fazio, V. M. (2011). The AOM/DSS murine model for the study of colon carcinogenesis: From pathways to diagnosis and therapy studies. *Journal of Carcinogenesis*, *10*, 9. http://doi.org/10.4103/1477-3163.78279

[30] Ke, X., Zhou, F., Gao, Y., Xie, B., Hu, G., Fang, W., … Sferra, T. J. (2013). Qing Hua Chang Yin exerts therapeutic effects against ulcerative colitis through the inhibition of the TLR4/NF-??B pathway. *International Journal of Molecular Medicine*, *32*(4), 926–930. http://doi.org/10.3892/ijmm.2013.1458

[31] Susaki, E. A., Tainaka, K., Perrin, D., Kishino, F., Tawara, T., Watanabe, T. M., … Ueda, H. R. (2014). Whole-brain imaging with single-cell resolution using chemical cocktails and computational analysis. *Cell*, *157*(3), 726–739. http://doi.org/10.1016/j.cell.2014.03.042

[32] Jun Abe , Aleksandra J. Ozga , JimSwoger, James Sharpe, Jorge Ripoll, J. V. S. (2016). Light sheet fluorescence microscopy for in situ cell interaction analysis in mouse lymph nodes. *Journal of Immunological Methods*.

[33] Wehrl, Bezrukov, Wieh, Lehnhoff, Fuchs, Mannheim, Quintanilla-Martinez, Kohlhofer, Kneilling, Pichler, S. A. (2015). Assessment of murine brain tissue shrinkage caused by different histological fixatives using magnetic resonance and computed tomography imaging